

Analysis of the regulatory mechanism of Two-pore channel 3
by membrane voltage and phosphoinositide

Hirazawa, Ki-ichi

The Graduate University for Advanced Studies, SOKENDAI
School of Life Science
Department of Physiological Sciences

Table of contents

Abbreviations	3
Summary	5
Introduction	8
Methods	11
Ethical approval	11
Molecular biology	11
Injection into <i>Xenopus</i> oocytes	11
Two-electrode voltage clamp recording of oocytes	12
Manipulation of PI(3,4)P ₂ level in <i>Xenopus</i> oocytes	12
Analysis of the MTSES-modification rate	13
Voltage clamp fluorometry	13
Data analysis and statistics	14
Three-dimensional structure modeling of <i>Xenopus tropicalis</i> TPC3	15
Results	16
Cys-accessibility analysis	16
Validation of D511C-TPC3 for the analysis of MTSES-modification	16
Analysis of the effect of PI(3,4)P ₂ binding on the 2 nd S4	17
Voltage clamp fluorometry	19
Screening of the optimal construct using Cys-based labeling of fluorophore	19
Examination of the voltage-dependent movement of the 1 st S4	20
Fluorescent labeling of the intracellular side of the 2 nd S4 using a fluorescent unnatural amino acid, Anap	21
Analysis of the effect of PI(3,4)P ₂ binding on the 2 nd S4 in VCF	22

Discussion	24
The unique remote control of the 2 nd S4 by the 1 st repeat in TPC3	24
The voltage dependent structural change of the 2 nd S4 of TPC3 inferred from this study	25
Limited structural change of the 1 st S4 of TPC family	27
The analysis of the effect of PI(3,4)P ₂ binding on the structural change of the 2 nd S4	27
The analysis of the structural dynamics of TPC using optical method	28
Concluding Remarks	30
Acknowledgements	31
Figures	32
References	55

Abbreviations

Anap	3-(6-acetylnaphthalen-2-ylamino)-2-aminopropanoic acid
Cav	voltage-gated Ca ²⁺ channel
cDNA	complimentary deoxyribonucleic acid
CiVSP	<i>Ciona intestinalis</i> voltage sensitive phosphatase
cRNA	complimentary ribonucleic acid
C-terminal	carboxy terminal
depo	depolarization
F change	change of fluorescent intensity
ΔF-V relationship	F change-voltage relationship
G-V relationship	conductance-voltage relationship
HEPES	4- (2-hydroxyethyl)-1-piperazineethanesulfonic acid
INPP4B	inositol polyphosphate 4-phosphatase type II
Kv	voltage-gated K ⁺ channel
MTSES	2-Sulfonatoethyl methanethiosulfonate sodium salt
NAADP	nicotinic acid adenine dinucleotide phosphate
Nav	voltage-gated Na ⁺ channel
NMDG	<i>N</i> -Methyl D-glucamine
N-terminal	amino terminal
PCR	polymerase chain reaction
PD	pore domain
PDB	protein data bank
PDBID	protein data bank ID
PIP ₂	phosphatidylinositol bisphosphate
PI(3,4)P ₂	phosphatidylinositol (3,4) bisphosphate

PI(3,4,5)P ₃	phosphatidylinositol (3,4,5) trisphosphate
PI(3,5)P ₂	phosphatidylinositol (3,5) bisphosphate
PI(4)P	phosphatidylinositol (4) phosphate
S.D.	standard deviation
S.E.M	standard error mean
S4	the 4 th helix
S6	the 6 th helix
TM	transmembrane
TPC	Two-pore channel
tRNA	transfer ribonucleic acid
VCF	voltage clamp fluorometry
VSD	voltage sensor domain
VSP	voltage sensitive phosphatase
V _{1/2}	membrane voltage for half maximum activation
WT	wild type
XtTPC3	<i>Xenopus tropicalis</i> TPC3

Summary

Two-pore channel (TPC) is a voltage-gated cation channel. A single polypeptide of TPC has 2 repeats of the canonical motif of voltage-gated cation channel, composed of the voltage sensor domain (VSD) and the pore domain (PD). The 4th helix in the VSD (S4) moves voltage dependently to open the gate of the channel. It is known that the 2nd VSD of TPC3 is responsible for the voltage sensing, whereas the 1st repeat has a phosphatidylinositol (3,4) bisphosphate (PI(3,4)P₂) binding site to potentiate the voltage dependence of TPC3.

This study aims to demonstrate the regulation of the voltage dependence of the 2nd S4 by the PI(3,4)P₂ binding to the 1st repeat in TPC3 from the point of view of the dynamic structural rearrangements.

Two approaches were used in this study, the cysteine (Cys)-accessibility analysis and the voltage clamp fluorometry (VCF) of *Xenopus tropicalis* TPC3 heterologously expressed in *Xenopus laevis* oocyte. In Cys-accessibility analysis, aspartate 511 at the extracellular side of the 2nd S4 was mutated to Cys (D511C-TPC3). The current of D511C-TPC3 was recorded using two-electrode voltage clamp, and sodium (2-sulfonatoethyl) methanethiosulfonate (MTSES), a Cys modifying reagent, was applied during the recording. The modification rate by MTSES was analyzed based on the MTSES-evoked current changes of D511C-TPC3, which reflects the movement of the 2nd S4. The effect of PI(3,4)P₂ binding on the modification rate was analyzed using a PI(3,4)P₂ binding deficient mutant (R187Q&D511C-TPC3) and a degradation enzyme of PI(3,4)P₂ (inositol polyphosphate 4-phosphatase type II, INPP4B). In VCF, specific residues in the 2nd S4 of TPC3 were labeled by fluorescent molecules to detect its movement based on the change of the fluorescent intensity (F change). The labeling at the extracellular side of the 2nd S4 was achieved using Cys-mutation and Cys-reactive Alexa Fluor™ 488 C5 Maleimide. The labeling at the intracellular side of the 2nd S4 was achieved using a genetic method for the incorporation of a fluorescent unnatural amino acid, 3-(6-acetylnaphthalen-2-

ylamino)-2-aminopropanoic acid (Anap). The current and fluorescent intensity of TPC3 were recorded simultaneously using two-electrode voltage clamp and fluorescent microscope, and the effect of PI(3,4)P₂ binding on the F change was analyzed.

In the Cys-accessibility analysis, the MTSES-modification rate of D511C-TPC3 increased in depolarized condition due to the movement of the 2nd S4. The MTSES-modification rate of D511C-TPC3 was larger than that of R187Q&D511C-TPC3. In addition, the modification rate of D511C-TPC3 was larger than that of D511C-TPC3 co-expressed with INPP4B. In VCF analysis, glutamine 507 was mutated to Cys (Q507C-TPC3) and labeled with the Alexa 488 fluorescent molecule. Q507C-TPC3 showed voltage dependent F change, but the amplitude of the F change was small (~0.6% at +180 mV). Serine 527 at the intracellular side of the 2nd S4 was mutated to Anap in S527Anap-TPC3. The construct showed larger voltage dependent F changes (~1.0% at +180 mV) compared to that of Q507C-TPC3, which enabled to examine the effect of PI(3,4)P₂ binding. The fluorescent intensity of S527Anap-TPC3 was decreased upon depolarization, and its F change was enhanced by the presence of PI(3,4)P₂. In addition, co-expression and activation of an exogenous voltage sensitive phosphatase (VSP), which transiently increases and then decreases the PI(3,4)P₂ level upon depolarization, caused a biphasic F change of S527Anap-TPC3. The fluorescent intensity was transiently decreased (then increased) during the transient production (then degradation) of PI(3,4)P₂ by VSP which indicated more (then less) depolarized-conformation of the 2nd S4.

As to the Cys-accessibility analysis, the voltage dependence of the MTSES-modification rate of D511C-TPC3 showed the structural rearrangement at around the 511 position upon depolarization. The larger MTSES-modification rate of the D511C-TPC3 bound to PI(3,4)P₂ suggests that the PI(3,4)P₂ binding to the 1st repeat of TPC3 potentiates the structural change of the 2nd S4 to the activated state. As to the VCF analysis, the small F change of Q507C-TPC3 labeled with the Alexa 488 suggests that the structural change at around the 507 position might be minor. The enhancement of the F change of S527Anap-TPC3 by the PI(3,4)P₂ binding

showed the potentiation of the structural change of the 2nd S4.

The effect of the PI(3,4)P₂ binding on the 2nd S4 was revealed through the analyses of the extracellular side (Cys-accessibility analysis) and the intracellular side (VCF) of the 2nd S4. Taken together, it was demonstrated that the PI(3,4)P₂ binding potentiates the structural rearrangements of the 2nd S4 and that the 2nd S4 of TPC3 integrates the information of the membrane voltage and the PI(3,4)P₂ binding to the 1st repeat to regulate the gating of the channel.

Introduction

Voltage-gated cation channels are membrane proteins which permeate specific ions in response to the change of the membrane potential (Hille, 2001). Voltage-gated cation channels are widely expressed in multiple tissues and organ, such as brain (Catterall, 2000) and play physiological roles such as generation of action potential. Due to their importance in physiology, many diseases, called as channelopathy, are caused by the pathological mutations of voltage-gated cation channels (Ashcroft, 2006).

Voltage-gated cation channels contain 6 transmembrane helices (6TM) (Yu and Catterall, 2004). The N-terminal 4 helices form voltage sensor domain (VSD), whereas the C-terminal 2 helices form pore domain (PD). The 4th helix (S4) in VSD has multiple positively charged residues (Arg, Lys). These positively charged residues enable S4 to move voltage dependently to gate the pore through the linker between S4 and S5 (Aggarwal and MacKinnon, 1996; Armstrong and Bezanilla, 1974; Long et al., 2005; Seoh et al., 1996). The voltage dependence of VSD is adjusted to respond suitably to the changes of the membrane voltage in the physiological range. On the other hand, PD has a gate and selectivity filter that determines the species of permeating ion (Doyle et al., 1998; Heinemann et al., 1992; MacKinnon, 1995). The coupling of VSD and PD enables the channel to open and close voltage dependently.

In view of the structural analysis, voltage-gated K⁺ channels (Kvs) are well-studied members of voltage-gated channels. Kvs have one repeat of 6TM in one polypeptide (monomer) (Papazian et al., 1987), and function as homo- or hetero-tetramers. On the other hand, eukaryotic voltage-gated Na⁺ and Ca²⁺ channels (Navs, Cavs) have 4 repeats of 6TMs within their single polypeptide (Mori et al., 1991; Noda et al., 1984). Two-pore channels (TPCs) have a specific feature that their single polypeptide has 2 repeats of 6TMs and function as homo- or hetero-dimer (Calcraft et al., 2009; Peiter et al., 2005). TPCs are considered to be an evolutionally intermediate form from one-repeat type Kvs and four-

repeats type Navs and Cavs (Amey et al., 2015; Penny et al., 2016; Rahman et al., 2014; Strong et al., 1993).

TPCs are chiefly localized on the intracellular organelle membranes (Xu and Ren, 2015). TPC family protein was initially found as a Ca^{2+} release channel which is located in endo/lysosome and activated by nicotinic acid adenine dinucleotide phosphate, NAADP (Calcraft et al., 2009). TPC family has 3 members, TPC1-3. The function of TPC1 and TPC2 have been extensively studied. They are localized in endo/lysosome and important for the maintenance of the ionic homeostasis of the intracellular organelle (Calcraft et al., 2009). TPC1 and TPC2 are important for autophagy (García-Rúa et al., 2016; Lin et al., 2015), nutrient sensing (Cang et al., 2013) and Ebola virus infection (Sakurai et al., 2015). Also, the regulators of TPC1 and TPC2 activity have been studied using patch clamp techniques including lysosomal patch clamp (Cang, Bekele, et al., 2014; Wang et al., 2012). For both channels, phosphatidylinositol (3,5) bisphosphate ($\text{PI}(3,5)\text{P}_2$), which is a kind of phospholipid localized on the endo/lysosomal membrane, is an activator. In addition to that, TPC1 is regulated by membrane voltage.

In contrast to TPC1, 2, there are limited reports about TPC3. As to the physiological function of TPC3, it is expressed in oocytes and fertilized eggs, and is important for correct proceeding of fertilization (Ramos et al., 2014). In the fertilized eggs of star fish with knockdown of TPC3, the fertilization envelope cannot be detached from the plasma membrane and the eggs show embryonic lethality. It was also revealed that TPC3 is localized not only on the intracellular membrane, but also on the plasma membrane. TPC3 was reported previously as a simple voltage-gated Na^+ channel with no sensitivity to PIP_2 (Cang, Aranda, et al., 2014). However, it was reported recently that TPC3 from *Xenopus tropicalis* is modulated by $\text{PI}(3,4)\text{P}_2$ and $\text{PI}(3,5)\text{P}_2$ (Shimomura and Kubo, 2019). When $\text{PI}(3,4)\text{P}_2$ binds to TPC3, its voltage dependence is potentiated to enable to open at less depolarized membrane voltages. The binding site of $\text{PI}(3,4)\text{P}_2$ is located in the former repeat (the 1st repeat) of two 6TMs

within a monomer of TPC3 (Fig. 1A). On the other hand, the voltage sensing is governed by the VSD in the 2nd repeat (the 2nd VSD, Fig. 1A), which was revealed by the charge-neutralizing experiment of the arginine residues of the 1st and the 2nd S4s (Dickinson et al., 2020). Therefore, it is suggested that the 1st and the 2nd repeats in TPC3 are coupled to enable the PI(3,4)P₂ binding to the 1st repeat to potentiate the voltage dependence of the 2nd VSD (Shimomura and Kubo, 2019). In more detail, it is possible that the PI(3,4)P₂ binding to the 1st repeat controls the voltage-dependent movement of the 2nd S4 in the 2nd repeat. In this thesis, this hypothetical mechanism is described as ‘remote control’.

In this study, the structural dynamics of the 2nd S4 was analyzed from the point of view of the regulation both by membrane voltage and PI(3,4)P₂, by Cys-accessibility analysis and voltage clamp fluorometry (VCF). Both methods have been used in many previous researches to track the structural change of the target proteins: Cys-accessibility (Baker et al., 1998; Hebeisen and Fahlke, 2005; Larsson et al., 1996; Li et al., 2010; Nakajo and Kubo, 2007; Wang et al., 2005), VCF (Kalstrup and Blunck, 2013; Mannuzzu et al., 1996; Nakajo and Kubo, 2014; Pless and Lynch, 2008; Sakata et al., 2016; Talwar and Lynch, 2015). Based on the results by these two methods, it was demonstrated that the movement of the 2nd S4 of TPC3 is facilitated by the conformational change of the distant 1st repeat caused by PI(3,4)P₂ binding.

Methods

Ethical approval

All animal experiments were approved by the Animal Care Committee of the National Institutes of Natural Sciences, and performed obeying its guidelines.

Molecular biology

The complementary DNA (cDNA) of TPC3 from *Xenopus tropicalis* (XtTPC3; XP_002940387) was subcloned into pGEMHE vector. The *Ciona intestinalis* voltage sensitive phosphatase (CiVSP) cDNA was provided by Prof. Okamura (Osaka University, Osaka, Japan). Site-directed mutagenesis was accomplished by a PCR-based method using PrimeSTAR Max DNA Polymerase and the In-Fusion HD Cloning Kit (Takara Bio), following the manufacturer's protocol. The plasmid sequences were confirmed by DNA sequencing. The cRNAs were transcribed using a mMMESSAGE mMACHINE T7 kit (Ambion; Life Technologies) from the linearized cDNA by Nhe1 restriction enzyme (Toyobo). The tRNA-synthetase/Anap-CUA encoding plasmid (pAnap) was obtained from Scripps Research Institute. Salt form of fluorescent unnatural amino acid, 3-(6-acetylnaphthalen-2-ylamino)-2-aminopropanoic acid (Anap, Futurechem) was dissolved in water and stocked at -20°C.

Injection into *Xenopus* oocytes

Females of *Xenopus laevis* for oocytes isolation were purchased from Hamamatsu Seibutsu Kyouzai (Japan). The oocytes were collected by surgical operation from frogs anesthetized by 0.15% tricaine. After the final collection, the frogs were humanely sacrificed by decapitation. The isolated oocytes were treated with 2 mg/ml collagenase (Sigma-Aldrich) for 6.5 h and stocked overnight or longer at 17 °C in frog Ringer's solution containing (in mM) 88 NaCl, 1 KCl, 2.4 NaHCO₃, 0.3 Ca(NO₃)₂, 0.41 CaCl₂, 0.82MgSO₄, and 15 HEPES, pH 7.6, with 0.1% penicillin–streptomycin (Sigma-Aldrich). The oocytes were then injected with 50 nl of cRNA solution and incubated at 17°C in frog Ringer's solution. Depending on the expression level of

the constructs, the amount of injected cRNAs of XtTPC3 per oocyte ranged 2.5 ~ 25 ng for Cys-accessibility analysis and 12.5 ~25 ng for voltage clamp fluorometry (VCF). In VCF using Anap, first, 0.5 ng pAnap was injected into nucleus of oocyte and the oocytes were incubated at 17 °C. On the next day, 25 pmol Anap was co-injected with cRNAs into cytoplasm in 50 nl solution. In the case of co-expression experiments with CiVSP, the mixture of 25 ng of XtTPC3 cRNA and 2.5 ng of CiVSP cRNA were injected. In the case of co-expression experiments with inositol polyphosphate 4-phosphatase type II (INPP4B), the mixture of 5 ng of XtTPC3 cRNA and 1.25 ng of INPP4B cRNA were injected. Currents were measured 4–6 days after injection, depending on the required current amplitude.

Two-electrode voltage clamp recording of oocytes

Currents were recorded under two-electrode voltage clamps using an OC-725C amplifier (Warner Instruments) and pClamp10.4 software (Molecular Devices). Data from the amplifier were digitized at 10 kHz through Digidata1440A (Molecular Devices). The resistance of the microelectrodes was 0.2–1.0 M Ω when filled with a solution of 3 M K-acetate and 10 mM KCl. The standard recording bath solution was ND-96, which contains (in mM) 96 NaCl, 2 KCl, 1.8 CaCl₂, 1 MgCl₂, and 5 HEPES, pH 7.4. Unless noted otherwise, the holding potential was at –40 mV. In Cys-accessibility analysis, after obtaining stable current by repeated depolarization pulses, 0.5 mM 2-Sulfonatoethyl methanethiosulfonate sodium salt (MTSES, Biotium) in ND-96 was applied to the bath by perfusion. Recordings were performed at room temperature.

Manipulation of PI(3,4)P₂ level in *Xenopus* oocytes

To control PI(3,4)P₂ concentration, voltage sensitive phosphatase (VSP) which is endogenously expressed in *Xenopus* oocyte was utilized (Kurokawa et al., 2012), except for the experiment using heterologous CiVSP. Long depolarization (e.g. +50 mV, ~10 sec) activates endogenous VSP and produces PI(3,4)P₂ at the plasma membrane. Therefore in this manuscript, ‘the absence of PI(3,4)P₂’ or ‘without PI(3,4)P₂’ means ‘before long depolarization’ whereas ‘the presence of PI(3,4)P₂’ or ‘with PI(3,4)P₂’ means ‘after long

depolarization’.

Analysis of the MTSES-modification rate

The current amplitude of D511C-TPC3 (a construct used in Cys-accessibility analysis) was not stable enough before MTSES application depending on oocyte batches, but the activation kinetics of TPC3 was rather stable. Thus, the kinetics was better for the analysis of the MTSES-modification. Each of the TPC3 current traces obtained by the repeated depolarization pulses was fitted by a double exponential function, and the activation rate was calculated. For Fig. 3C, the rate constant of the slow component was used for the analysis, because it was more stable during recoding than that of the fast component in this experiment (the contribution of the slow component was ~40%). For Fig. 4D and Fig. 5C, the rate constant of the fast component was more stable in this experiment (the contribution of the fast component was 60~80%) and used for the analysis. MTSES-induced changes in the TPC3 activation rate were obtained by subtracting the activation rate just before MTSES application ($\text{rate}(t=0)$) from the activation rates recorded at each time point ($\text{rate}(t)$). The obtained values were then normalized to the calculated maximum increase in the activation rate ($\text{rate}(t=\infty)-\text{rate}(t=0)$), to show clearly the difference in the modification rates between different conditions (e.g. protocols, constructs). After plotting the normalized value as a function of time, MTSES-modification rate was obtained by fitting the plots using single exponential functions.

Voltage clamp fluorometry

In the case of VCF using Alexa Fluor™ 488 C5 Maleimide (Thermo Fisher Scientific), oocytes with expression of TPC3 constructs (shown in Figs. 6, 8) were pre-incubated in high K^+ buffer which contains (in mM) 98 KCl, 1.8 CaCl₂, 1 MgCl₂, and 5 HEPES, pH 7.4. for 30 min at 4 °C to activate endogenous VSP (described above). After that incubation, oocytes were labeled in ND-96 with 100 μM Alexa Fluor™ 488 C5 Maleimide (Thermo Fisher Scientific). In ND-96, the membrane potential is expected to be depolarized to the reversal potential of Na^+ (~80 mV) due to the activity of the expressed TPC3 after long depolarization during the pre-

incubation which could be optimal to label the S4. After that, the oocytes were rinsed and stored in NMDG buffer which contains (in mM) 20 NaCl, 76 *N*-Methyl *D*-glucamine (NMDG), 2 KCl, 1.8 CaCl₂, 1 MgCl₂, and 5 HEPES, pH 7.4.

The fluorometric recordings were performed with an upright fluorescence microscope (Olympus BX51WI) equipped with a water immersion objective lens (Olympus XLUMPLFLN 20x/1.00) to collect the emission light from the oocytes. The excitation light from xenon arc lamp (L2194-01, Hamamatsu Photonics) was applied through a band-pass excitation filter (465-495 nm for Alexa488, 330-360 nm for Anap). To minimize the photobleaching during recording, the intensity of the excitation light was decreased to 1.5 or 6.0% with ND filters (U-25ND6, U-25ND25 Olympus) depending on the intensity of the emitted fluorescence. The emission light was passed through the band pass filter: for Alexa488, 510 -550 nm (U-MWIBA3, Olympus); for Anap, 420-460 nm and 460-520 nm (Brightline, Semrock) (Lee et al., 2009; Sakata et al., 2016). The emission signals were detected by one (for Alexa) or two (for Anap) photomultipliers (H10722-110; Hamamatsu Photonics). The detected fluorescent intensities and TPC3 currents were acquired by the Digidata 1332 (Axon Instruments) and pClamp 10.3 software (Molecular devices) at 20 kHz. To improve the signal to noise ratio, VCF recordings were repeated 3~20 times for each sample. The averaged data were used for data presentation and analysis. A slow bleaching was adjusted by assuming that the decrease until each voltage step pulse was linear.

Data analysis and statistics

Electrophysiological data were analyzed using Clampfit 10.7 (Molecular Devices) and Igor Pro (WaveMetrics). Tail current amplitude elicited by +60 mV after step pulse was used to obtain conductance-voltage (G-V) relationship. To obtain the change of fluorescent intensity-voltage (ΔF -V) relationship, the changes of the intensity from the baseline intensity caused by the step pulse were presented as percent of the baseline intensity. The G-V and ΔF -V relationships were calculated by fitting to a sigmoidal function, G or $\Delta F = \max / (1 + \exp((V_{1/2} -$

$V/k)) + \text{base}$, where G indicates the conductance, and ΔF indicates the change of the fluorescent intensity. V is the membrane voltage, and $V_{1/2}$ is the membrane voltage for half maximum activation. k is slope factor. The normalized G/G_{max} and $\Delta F/\Delta F_{\text{max}}$ were plotted as functions of membrane voltage. Data are presented as mean \pm S.D. unless otherwise noted. Student's t-test was used for statistical comparison. $p < 0.05$ was considered statistically significant. *, ** denote values of $p < 0.05$, 0.01 , respectively. All the statistical analyses were performed using Excel (Microsoft) and the statistical graphs were drawn using Igor Pro (WaveMetrics).

Three-dimensional structure modeling of *Xenopus tropicalis* TPC3

Homology structure modeling was performed using a web-based environment for protein structure homology modeling SWISS-MODEL (Arnold et al., 2006; Biasini et al., 2014) based upon sequence alignment of amino acids of XtTPC3 (XP_002940387) and crystal structure of *Mus musculus* TPC1 (PDBID: 6C9A) (She et al., 2018) or *Arabidopsis thaliana* TPC1 (PDBID: 5E1J) (Guo et al., 2016). All the structure figures presented in this study were generated using PyMOL molecular graphics system ver. 1.7.x (Schrödinger, LLC). The binding model of PI(3,4)P₂ at the 1st repeat of TPC3 (Fig. 4A) was provided by Dr. Shimomura in our laboratory.

Results

Cys-accessibility analysis

Validation of D511C-TPC3 for the analysis of MTSES-modification

The aim of this study is to examine the possibility that PI(3,4)P₂ binding to the 1st repeat of TPC3 affects the 2nd S4. The movement of the 2nd S4 was evaluated by measuring the modification rate of the introduced cysteine residue (Cys) in the 2nd S4 by MTSES, which covalently modifies Cys, in *Xenopus* oocytes heterologous expression system. The principle of this method is as reported previously (Nakajo and Kubo, 2007). Upon application of MTSES to TPC3 with a Cys residue in the 2nd S4 that is important for voltage sensing, MTSES-modification at the introduced Cys could affect the voltage dependence and the currents of TPC3 (Fig. 1B). The rate of this modification depends on the extent of exposure of the introduced Cys to the bath solution. Therefore, the PI(3,4)P₂ binding-induced change of the movement of the 2nd S4 could be detected as the difference in the modification rates between in the absence and presence of PI(3,4)P₂.

As the first step, the optimal position of the Cys-introduction in TPC3 was searched. D511C mutation at the extracellular side of the 2nd S4 shifted the voltage dependence of TPC3 to the depolarized direction (the membrane voltages for half maximum activation ($V_{1/2}$) of wild type (n = 3): 61.7 ± 19.1 mV; D511C (n = 3): 112.1 ± 2.5 mV, slope factor of wild type (n = 3): 25.3 ± 0.2 mV; D511C (n = 3): 25.2 ± 1.4 mV, Fig. 1D). The covalent modification by a negatively charged MTSES at the neutral Cys511 could mimic the original negative charge of D511 and restore the wild type property. Therefore, D511C-TPC3 was chosen for the MTSES Cys-modification analysis. The MTSES effects were investigated in the presence of PI(3,4)P₂, whose concentration was increased by applying long depolarization (+50 mV) in advance using the activity of the endogenous voltage sensitive phosphatase (Methods). MTSES application to D511C-TPC3 showed current increase (Fig. 2A), in contrast to that to wild type TPC3 which

showed no apparent change (Fig. 2A). The conductance-voltage relationship of D511C-TPC3 was shifted to the hyperpolarized direction by MTSES-modification ($V_{1/2}$ of without MTSES (n = 4): 128.8 ± 2.2 mV; with 0.5 mM MTSES (n = 6): 86.3 ± 19.6 mV, slope factor of without MTSES (n = 4): 27.9 ± 4.8 mV; with 0.5 mM MTSES (n = 6): 45.6 ± 18.6 mV, Fig. 2B), which explains the MTSES-induced current increase at constant voltage.

To examine the voltage dependence of the modification rate (Fig. 3A), two kinds of protocols were used (Fig. 3B). One is “less depolarized protocol” in which 0.1 sec depolarization in every 1.6 sec is applied repeatedly in the presence of MTSES. Another one is “more depolarized protocol” with 0.3 sec depolarization in every 1.6 sec. In both protocols, D511C-TPC3 showed MTSES-evoked current increase. To evaluate the MTSES-modification rate, the activated TPC3 current was fitted by a double exponential function and the two activation rates for each pulse were calculated. Those of the slow component were plotted as a function of time from the starting point of MTSES application (Fig. 3C). In both protocols, the activation rates were increased by the MTSES-modification. After normalization (described in Methods), the MTSES-modification rates were calculated by single exponential fitting (Fig. 3C). In more depolarized protocol, MTSES-modification rate was larger than that in less-depolarized one (Fig. 3D). This result indicates that depolarization-evoked movements of the 2nd S4 induced the exposure of D511C to the external bath solution, resulting in the faster MTSES-modification in more depolarized protocol than that in less depolarized one (Fig. 3A). These results show that using D511C-TPC3 and MTSES, the structural change of the 2nd S4 can be detected; faster modification rate indicates more depolarized conformation of the 2nd S4. The homology structure models of the resting and activated TPC3 are shown in Fig. 3E to show the difference of the location of D511 depending on the states.

Analysis of the effect of PI(3,4)P₂ binding on the 2nd S4

Next, the effect of PI(3,4)P₂ binding on MTSES-modification rate of D511C-TPC3 was

examined. For this experiment, it is necessary to control the level of PI(3,4)P₂. Long depolarization activates oocyte-endogenous VSP which produces PI(3,4)P₂ (Methods). Therefore, the difference of the MTSES-modification rates before and after long depolarization was analyzed. However, the repeated depolarizations to detect MTSES-modification activated endogenous VSP and resulted in gradual increase of PI(3,4)P₂ concentration even in the ‘without PI(3,4)P₂ (before long depolarization)’ condition, which made it difficult to separate the MTSES-modification and PI(3,4)P₂-induced potentiation. To overcome this problem, an alternative approach to use R187Q&D511C-TPC3 mutant was taken. It was reported that the mutant cannot bind to PI(3,4)P₂ efficiently even after long depolarization, because of the lack of a positive charge at 187 which is indispensable for the PI(3,4)P₂ binding (Shimomura and Kubo, 2019) (Fig. 4A). Thus, the MTSES-modification rates were compared between D511C-TPC3 and R187Q&D511C-TPC3 in the presence of PI(3,4)P₂ using the same protocol. The protocol used here contains depolarization pulse at +135 mV, which is expected to discriminate the activation states of D511C-TPC3 and R187Q&D511C-TPC3 effectively based on the conductance-voltage (G-V) relationships ($V_{1/2}$ of D511C-TPC3 (n = 10): 100.5 ± 4.8 mV; R187Q&D511C-TPC3 (n = 8): 180.0 ± 50.1 mV, slope factor of D511C-TPC3 (n = 10): 22.9 ± 2.8 mV; R187Q&D511C-TPC3 (n = 8): 46.1 ± 20.9 mV, Fig. 4B). Both constructs showed MTSES-dependent current increase (Fig. 4C) and accelerated the activation of TPC3 (Fig. 4D). MTSES-modification rate of D511C-TPC3 was significantly larger than that of R187Q&D511C-TPC3 (Fig. 4E). This result indicates that the 2nd S4 of D511C-TPC3 is more frequently exposed to the extracellular side by +135 mV depolarization than that of R187Q&D511C-TPC3. This difference could be attributed to the reduced PI(3,4)P₂ binding in R187Q&D511C-TPC3.

To further prove the effect of PI(3,4)P₂ binding on the MTSES-modification of D511C-TPC3, another approach was tested using PI(3,4)P₂ degradation enzyme, INPP4B (Fruman et al., 2017). INPP4B is a phosphatase that specifically dephosphorylates PI(3,4)P₂. Therefore,

heterologous expression of INPP4B is expected to decrease the concentration of PI(3,4)P₂ in oocytes even after long depolarization stimulus. D511C-TPC3 was co-expressed with or without INPP4B. First, after long depolarization, G-V relationships were analyzed in both conditions, which showed a positive shift by INPP4B ($V_{1/2}$ of D511C-TPC3 (n = 6): 99.5 ± 3.4 mV; D511C-TPC3+INPP4B (n = 6): 140.4 ± 3.5 mV, slope factor of D511C-TPC3 (n = 6): 27.4 ± 2.9 mV; D511C-TPC3+INPP4B (n = 6): 27.4 ± 2.4 mV, Fig. 5A). The same protocol as the one in the comparison between D511C-TPC3 and R187Q&D511C-TPC3 (+135 mV depolarization) was used. INPP4B co-expression decreased the MTSES-modification rate most likely through degradation of PI(3,4)P₂, indicating that depletion of PI(3,4)P₂ induced the structure of the 2nd S4 in more downward state (Figs. 5B-D). This result goes well with that of the comparison between D511C-TPC3 and R187Q&D511C-TPC3, which showed that PI(3,4)P₂ binding can potentiate the upward translocation of the 2nd S4.

Voltage clamp fluorometry

To detect structural changes of membrane proteins, voltage clamp fluorometry (VCF) is a useful method in which specific amino acid can be labeled by fluorescent molecule and the changes of its fluorescent intensity (F changes) report local structural change (Mannuzzu et al., 1996; Nakajo and Kubo, 2014; Pless and Lynch, 2008; Talwar and Lynch, 2015). F change can be caused by the changes of the chemical environment surrounding the fluorescent molecule. Based on the canonical model of the S4 movement, the extracellular and intracellular sides of the 2nd S4 are expected to change their chemical environment upon activation, e.g. from the lipid bilayer phase to the water phase or vice versa (Fig. 6A). Therefore, the structural rearrangements of the 2nd S4 was investigated by VCF of TPC3 with fluorescent labeling at these regions of the 2nd S4.

Screening of the optimal construct using Cys-based labeling of fluorophore

Cys-mutation at the aimed positions followed by covalent labeling using maleimide-conjugated fluorescent dye is a canonical method for VCF (Mannuzzu et al., 1996; Nakajo and Kubo, 2014; Pless and Lynch, 2008; Talwar and Lynch, 2015). Because the fluorescent molecule is basically impermeable to cell membrane, this labeling method is applicable only to the extracellular side. Residues at the extracellular side of the 2nd S4 were tested as the candidates for labeling sites (Fig. 6B). These residues were mutated to Cys one at a time and the constructs were expressed in *Xenopus* oocyte. After incubation of the oocytes with Alexa Fluor™ 488 C5 Maleimide in depolarized condition for efficient labeling (Methods), TPC3 current and F change were simultaneously recorded (Fig. 6C). Many constructs showed TPC3 current at +180 mV (Fig. 6C). The percentage of oocytes showing apparently detectable F changes (>0.2%) is as follows for each construct (% of the number of the oocytes showing F changes/total oocytes (n = 6 ~ 11)): S497C (0), L498C (0), K499C (0), G502C (17), Q503C (0), S506C (78), Q507C (91). Especially, Q507C-TPC3 showed apparent F changes with a high reproducibility compared to the others. The G-V and ΔF -V relationships of Q507C-TPC3 were obtained in the presence of PI(3,4)P₂ (Figs. 7A-C). By fitting the plot using a sigmoidal function (Methods), V_{1/2} was obtained (G-V: 91.9 ± 6.7 mV; ΔF -V: 99.2 ± 8.8 mV (n = 10)). Slope factor was also obtained (G-V: 24.8 ± 3.7 mV; ΔF -V: 22.1 ± 4.1 mV (n = 10)). Although the obtained F change using Cys-TPC3 construct was reproducible, the amplitude of the F change (~0.6%) was not sufficient to proceed to further analysis in the absence of PI(3,4)P₂, possibly due to the decreased F change in this condition.

Examination of the voltage-dependent movement of the 1st S4

In addition to the 2nd S4, TPC3 has the 1st S4. As the 1st S4 also has positively charged amino acid residues within its transmembrane segment (Fig. 8A), it is possible that the 1st S4 also shows voltage-dependent movement. Residues at the extracellular side of the 1st S4 were mutated to Cys one at a time and labeled by Alexa dye (Fig. 8A), and tested by VCF after long

depolarization. Most constructs showed voltage-dependent TPC3 current, while no construct of the 1st S4 showed voltage-dependent F change in the same criteria as the 2nd S4 (Fig. 8B; the percentage of the number of the oocytes showing F changes/total oocytes (n = 4 ~ 7) was 0% in A157C, L158C, A161C, S165C, V166C). Simultaneous recordings of the oocytes expressing S506C- or Q507C-TPC3 from the same batches showed detectable F changes (the percentage of the oocytes (n = 2, 3) showing F change was 100% for both constructs). Based on this result, it was suggested that the 1st S4 doesn't show remarkable voltage-dependent movement in contrast to the 2nd S4.

Fluorescent labeling of the intracellular side of the 2nd S4 using a fluorescent unnatural amino acid, Anap

The intracellular side of the 2nd S4 was also tested as candidates for labeling. As Cys-based labelling is not applicable to the intracellular side, a fluorescent unnatural amino acid, Anap, was used. Anap is incorporated during protein translation (Lee, Guo et al. 2009), and thus it can label at any position (Fig. 9). On the 1st day, pAnap, a plasmid which encodes tRNA for Anap and Anap-tRNA synthetase, is injected into the nucleus of oocyte. On the next day, Anap and cRNA of TPC3 are injected into the cytosol. Expressed synthetase will catalyze the synthesis of tRNA loaded with Anap (Anap-tRNA) specifically. Anap-tRNA recognizes UAG (amber) codon in the cRNA and makes Anap incorporated to the polypeptide chain. Thus, by mutating the DNA sequence of the residue at aimed position to TAG, Anap can be incorporated.

The Anap labeling sites were screened at around the intracellular side of the 2nd S4 (Figs. 10A, B). Some constructs showed voltage-dependent TPC3 current. Only S527Anap-TPC3 showed voltage-dependent F change in which the fluorescent intensity decreases upon depolarization (% of the number of the oocytes showing F changes/total oocytes (n = 9 ~ 13): D526Anap (0), S527Anap (92), I528Anap (0), R530Anap (0)). The percentage of the F change of S527Anap-TPC3 at +180 mV was ~1% (Fig. 10B), which was larger than those of the Cys-

based constructs (~0.6%). The G-V and ΔF -V relationships were obtained in the presence of PI(3,4)P₂ (Figs. 11A-C, V_{1/2} of G-V: 93.5 ± 11.9 mV; ΔF -V: 119.0 ± 45.3 mV (n = 7), slope factor of G-V: 30.2 ± 4.2 mV; ΔF -V: 34.1 ± 16.5 mV (n = 7)). The homology structure models of the resting and activated states suggested that S527 is located near the border of the plasma membrane in the resting state, and approaches to the lipid bilayer when activated (Fig. 11D), which is considered to induce the F change.

Analysis of the effect of PI(3,4)P₂ binding on the 2nd S4 in VCF

As the F change from S527Anap-TPC3 is reproducible and relatively large, we analyzed the effect of PI(3,4)P₂ binding on the F change. The determination of ΔF -V relationship before long depolarization (without PI(3,4)P₂) was again difficult due to the small F change at the low membrane voltages. To examine the effect of PI(3,4)P₂, the F changes in the absence and presence of PI(3,4)P₂ were compared at a single depolarized membrane voltage. Short depolarization pulse at +80 mV was repeated before and after application of long depolarization which increased PI(3,4)P₂ (Fig. 12A). The obtained TPC3 current was slightly potentiated in the presence of PI(3,4)P₂. Furthermore, although there was almost no F change in the absence of PI(3,4)P₂, a significant voltage-dependent F change was detected at the same voltage in the presence of PI(3,4)P₂. The F changes were significantly larger in the presence of PI(3,4)P₂ than those in the absence (0.16 ± 0.09% in the absence of PI(3,4)P₂ vs 0.29 ± 0.15% in the presence of PI(3,4)P₂ (n = 9), Fig. 12B). These results show that the binding of PI(3,4)P₂ can potentiate the voltage-dependent structural change of the 2nd S4.

Next, to manipulate the concentration of PI(3,4)P₂ more drastically, exogenous VSP was co-expressed (Fig. 13A). When VSP derived from *Ciona intestinalis* (CiVSP) is heterologously expressed in oocytes, it dephosphorylates PI(3,4,5)P₃ at the plasma membrane to produce PI(3,4)P₂ upon depolarization (Grimm and Isacoff, 2016; Kurokawa et al., 2012). However, produced PI(3,4)P₂ is also a substrate for CiVSP, then CiVSP dephosphorylates PI(3,4)P₂ to

PI(4)P. Therefore, upon long depolarization, the concentration of PI(3,4)P₂ will transiently increase, and then decrease in the oocyte with heterologous CiVSP. VCF analysis of the oocyte expressing S527Anap-TPC3 and CiVSP was performed (Fig. 13B). By the long depolarization, transient production and following degradation of PI(3,4)P₂ were expected to occur. Consistent with the dynamic change of PI(3,4)P₂ concentration, inward current of S527Anap-TPC3 transiently increased and then decreased (Fig. 13B). The fluorescent intensity of S527Anap-TPC3 also showed a biphasic change in accordance with the expected change of PI(3,4)P₂ concentration (Fig. 13B). The time scale of the dynamic changes of both current and fluorescent intensity is in a similar range to that of the CiVSP-induced change of the PI(3,4)P₂ concentration determined by fluorescence-based PI(3,4)P₂ sensor in previous studies (Grimm and Isacoff, 2016; Kurokawa et al., 2012; Shimomura and Kubo, 2019). Furthermore, during the transient increase in PI(3,4)P₂ concentration, the fluorescent intensity decreases which indicates the transition to the depolarized conformation of the 2nd S4. Then, as PI(3,4)P₂ is dephosphorylated, the fluorescent intensity reverts close to the base line level which indicates the transition to the hyperpolarized conformation of the 2nd S4. Taken together, by the co-expression experiment with CiVSP, it was again shown that the binding of PI(3,4)P₂ can potentiate the voltage-dependent structural change of the 2nd S4.

Discussion

Two kinds of methods were used in this study to examine the remote control of the structural rearrangement of the 2nd S4 by PI(3,4)P₂ binding to the 1st repeat in TPC3. One is the Cys-accessibility analysis based on the covalent modification of Cys residue by MTSES. Another is the VCF in which the 2nd S4 is labeled by fluorescent molecules. These analyses brought following findings. (1) The MTSES-modification rate of D511C-TPC3 showed voltage dependence due to the structural change of the 2nd S4 (Fig. 3). (2) The MTSES-modification of D511C-TPC3 was accelerated by the PI(3,4)P₂ binding (Figs. 4, 5). (3) Some TPC3 constructs with fluorescent labeling at both the extracellular side and the intracellular side of the 2nd S4 showed voltage-dependent changes of the fluorescent intensity which report the structural changes of the 2nd S4 (Figs. 6, 10). (4) TPC3 constructs with fluorescent labeling at the extracellular side of the 1st S4 showed no voltage-dependent change of the fluorescent intensity (Fig. 8). (5) The change of the fluorescent intensity of S527Anap-TPC3 was potentiated by PI(3,4)P₂ binding (Fig. 12). (6) The rapid and biphasic change of PI(3,4)P₂ concentration induced by the co-expression of exogenous CiVSP resulted in a biphasic change of the fluorescent intensity of S527Anap-TPC3 (Fig. 13). Taken together, it was concluded that PI(3,4)P₂ binding to the 1st repeat of TPC3 can potentiate the voltage-dependent structural change of the 2nd S4 (Fig. 14A).

The unique remote control of the 2nd S4 by the 1st repeat in TPC3

The aim of this study is to prove the remote control of the voltage-dependent structural change of the 2nd S4 by PI(3,4)P₂ binding to the 1st repeat. By the analyses of Cys-accessibility and VCF, it was revealed that PI(3,4)P₂ binding to the 1st repeat can potentiate the voltage dependence of TPC3 activation through the modulation of the structural change of the 2nd S4. This potentiation of the voltage dependence by PI(3,4)P₂ binding is specific feature of TPC3

among TPC family (Shimomura and Kubo, 2019). TPC1 has a voltage dependence for activation, and the current amplitude can be increased by PI(3,5)P₂ binding to the 1st repeat. However, its voltage dependence cannot be potentiated by PI(3,5)P₂ (She et al., 2018). TPC2 doesn't show voltage dependence for its activation, while it can be gated simply by PI(3,5)P₂ binding to the 1st repeat (Wang et al., 2012). The possible reason of this specificity of the remote control of voltage dependence by PI(3,4)P₂ binding in TPC3 is the inter-repeat linking between the 1st and the 2nd repeat (Shimomura and Kubo, 2019). It is located between the 1st S6 (6th transmembrane helix) and the 2nd S6 of *Xenopus* TPC3 (Fig. 14B), composed of hydrophilic and electrostatic interactions of Tyr293 (1st S6), Arg297 (1st S6) and Glu665 (2nd S6). As the disruption of this interaction by point mutation abolishes the potentiation of the voltage dependence of TPC3 by PI(3,4)P₂, the remote control is thought to be mediated by this inter-repeat interaction (Shimomura and Kubo, 2019). As this link is lacked in mouse TPC1 (Fig. 14B), which has Phe, Asn, and Glu at the corresponding positions to Tyr293, Arg297 and Glu665, respectively, the difference can explain the TPC3 specificity of this remote control.

The physiological relevance of this remote control remains to be elucidated. However, given the Na⁺ selectivity which causes strong depolarization and the lack of inactivation of TPC3 (Cang, Aranda, et al., 2014), the opening of TPC3 needs to be strictly regulated to avoid toxic long depolarization. Thus, the remote control might be a safe guard which enables TPC3 to open only when both PI(3,4)P₂ and depolarization stimulate TPC3. Considering the expression of TPC3 in oocytes and fertilized eggs and its importance for fertilization (Ramos et al., 2014), it is possible that this remote control tightly regulates the physiological activation of TPC3 during fertilization, and thus it is evolutionally conserved.

The voltage-dependent structural change of the 2nd S4 of TPC3 inferred from this study

A canonical voltage-dependent activation of S4 is considered to be accompanied with a sliding and/or rotating motion, which makes the extracellular side of the S4 exposed to the

extracellular solution (Larsson et al., 1996; Yang et al., 1996). Consistent with this movement, the MTSES-modification rate at D511C showed a voltage dependence in TPC3 (Figs. 3C, D). This is also consistent with the homology structure models of the 2nd VSD of TPC3 in the resting and activated states (Fig. 3E). D511 is further away from the membrane in the activated state compared to the resting state. Thus, this difference of the location of D511 depending on the state of the 2nd S4 can explain the observed voltage dependence of the MTSES-modification rate.

TPC3 constructs for Cys-based fluorescent labeling at the extracellular side of the 2nd S4 showed voltage-dependent F changes. A successful detection of the F changes at the extracellular side of S4 (Fig. 6C) is consistent with the reports of VCF experiments on other voltage-gated cation channels (Blunck et al., 2004; Cha and Bezanilla, 1997; Nakajo and Kubo, 2014; Vaid et al., 2009). However, the percentage of the obtained F change (less than 1%) from TPC3 constructs in this study was far lower than the F changes (~20%) from other voltage-gated cation channels (Cha and Bezanilla, 1997). There are possible reasons of the small F change, including lower expression level of the TPC3 constructs and/or lower efficiency of labeling by fluorophore. The other possibility is that the structural change at the extracellular side of the 2nd S4 of TPC3 is intrinsically minor and therefore doesn't cause large chemical environmental change of the fluorophore. Thus, it is possible that the 2nd S4 of TPC3 undergoes different conformational change upon depolarization compared to other canonical S4.

In the VCF using Anap labeling, residues at the intracellular side of the 2nd S4 were examined. Among these constructs, only S527Anap-TPC3 showed voltage-dependent F change and its percentage (~1%) was larger than those from the extracellular labeling constructs. S527 is located at the very end of the 2nd S4 helix in the homology models (Fig. 11D). Therefore, it is possible that the dihedral angle of the peptide backbone at S527Anap is dynamically changed during the 2nd S4 movement, which might be one possible reason of the relatively large F change of S527Anap-TPC3.

The G-V and ΔF -V relationships of S527Anap-TPC3 are almost indistinguishable (Fig. 11C). Generally, ΔF -V of the S4 helix is in more hyperpolarized voltage than G-V (Kalstrup and Blunck, 2013), because movements of multiple S4s and the final state transition are required to open the gate. The lack of the difference between the G-V and ΔF -V relationships in TPC3 might indicate that the structural rearrangement of only one of the two 2nd S4s in TPC3 homodimer is sufficient to open the gate.

Limited structural change of the 1st S4 of TPC family

In addition to the 2nd S4, the 1st S4 of TPC3 also has positive charges within its transmembrane segment. Thus, it is natural to speculate that the 1st S4 can also move voltage dependently. However, all of the TPC3 constructs tested with fluorescent labeling at the extracellular side of the 1st S4 didn't show any clear voltage-dependent F changes (Fig. 8), which is in high contrast to those of the 2nd S4. This result suggests that the 1st S4 doesn't move voltage dependently. This is consistent with the result of charge neutralizing mutation study of the arginine residues of the 1st S4, showing no significant effect on voltage dependence of TPC1 and TPC3 (Dickinson et al., 2020; She et al., 2018). Furthermore, this is also consistent with the structural study of TPCs, showing that the 1st S4 has a different structure from the canonical S4 (She et al., 2019). Therefore, the 1st S4 of TPC family member is considered to have limited roles in voltage sensing.

The analysis of the effect of PI(3,4)P₂ binding on the structural change of the 2nd S4

The analysis in the absence of PI(3,4)P₂ was challenging in both Cys-accessibility and VCF analyses, as described in the following. Therefore, to conclude the effect of PI(3,4)P₂ binding on the structural change of the 2nd S4, four different approaches were taken. (1) Repeated depolarization pulses, which are necessary to detect MTSES-modification of TPC3 current, cause gradual accumulation of PI(3,4)P₂ due to the activation of the endogenous VSP activity

of oocytes. To overcome this difficulty, R187Q mutation was used. (2) In another experiment to overcome the problem described above, INPP4B was used to deplete PI(3,4)P₂, maintaining TPC3 protein intact. (3) In VCF, the determination of the ΔF -V relationship of S527Anap-TPC3 in the absence of PI(3,4)P₂ still remains challenging because of the smaller F change than that in the presence of PI(3,4)P₂. To reveal the effect of PI(3,4)P₂ on F change, weak depolarization pulses (+80 mV) were repeated before and after long depolarization. (4) CiVSP was used to manipulate the concentration of PI(3,4)P₂ dynamically. It was hard to detect the F change during long depolarization, possibly due to the low PI(3,4)P₂ productivity of endogenous VSP of oocytes. The heterologous expression of CiVSP enabled the rapid and large change of the PI(3,4)P₂ concentration, resulting in the clear detection of F changes of S527Anap-TPC3 during long depolarization.

Cys-accessibility analysis indicates that PI(3,4)P₂ binding causes more frequent exposure of the extracellular side of the 2nd S4 to the bath solution. VCF analysis of S527Anap also showed the potentiation of the translocation of the intracellular side of the 2nd S4 by PI(3,4)P₂ binding. Such movements are consistent with the direction of the canonical voltage-dependent movement. Taken together, it is straightforward to speculate that the PI(3,4)P₂ binding increases the probability of usual voltage-dependent S4 movement, rather than causes remarkable mode shift. In other words, it is conceivable that the PI(3,4)P₂ binding to the 1st repeat of TPC3 potentiates the structural rearrangements of the 2nd S4 to the activated state (Fig. 14A).

The analysis of the structural dynamics of TPC using optical method

High resolution structures of TPC family have been revealed recently using X-ray crystal structure analysis (Guo et al., 2016; Guo et al., 2017; Kintzer et al., 2018; Kintzer and Stroud, 2016) and single particle structure analysis using cryo-electron microscopy images (Kintzer et al., 2018; She et al., 2018; She et al., 2019). Although structures of TPCs in multiple states (e.g. PIP₂ bound and apo) have already been reported, the dynamic information of TPC structure

detected over time is still lacking. Here, using VCF, the dynamic structural change of the 2nd S4 of TPC3 over time was tracked, showing the effect of PI(3,4)P₂ binding on it. This study revealed the difference of the structural dynamics of the 2nd S4 between apo and PI(3,4)P₂ bound states, which has not been shown in the structure analyses. This is the first study of the optical detection of the structural change of TPC family protein, and thus it would serve as a framework of the analysis of the dynamic aspects of the TPC structure.

Concluding remarks

To reveal the effect of PI(3,4)P₂ binding on the structural change of the 2nd S4, two kinds of methods were used: Cys-accessibility analysis and voltage clamp fluorometry. The experiments using these methods brought following findings.

(1) The MTSES-modification rate of D511C-TPC3 reported the structural change of the 2nd S4. The modification rate was larger when PI(3,4)P₂ binds to the 1st repeat of TPC3 than when unbound, showing the potentiation of the structural change of the 2nd S4.

(2) The fluorescent labeling at the extracellular side of the 2nd S4 reported the voltage-dependent movement of the 2nd S4 of TPC3.

(3) The fluorescent labeling at the intracellular side of the 2nd S4 reported the voltage-dependent movement of the 2nd S4 of TPC3. The change of the fluorescent intensity was enhanced when PI(3,4)P₂ binds to the 1st repeat of TPC3.

(4) Taken together, it was shown that the 1st repeat of TPC3 is coupled to the 2nd repeat to enable the PI(3,4)P₂ binding to the 1st repeat to remotely regulate the structural change of the 2nd S4. Therefore, the 2nd S4 of TPC3 can integrate the information of the membrane voltage and the PI(3,4)P₂ binding to the 1st repeat. This inter-repeat coupling is specific to TPC3, which might be involved in the physiological function specific to TPC3.

These findings will give new insights into the functioning mechanisms of voltage-gated cation channels.

Acknowledgements

First of all, I am extremely grateful to Prof. Yoshihiro Kubo and Dr. Takushi Shimomura for the continuous support of my Ph.D study, for their patience, motivation, and immense knowledge. Thanks to their guidance, I could accomplish this research and writing of this thesis.

I would like to thank Prof. Yasushi Okamura for generously providing cDNA encoding CiVSP for VCF experiment.

I would like to thank Dr. Michihiro Tateyama, Dr. I-Shan Chen and Dr. Rizki Tsari Andriani in Kubo lab for their insightful comments and continuous encouragements. I also would like to thank former Kubo lab member Dr. Shinichiro Kume for his support with kindness and important discussions. I would like to thank my fellow lab member Ms. Liu Chang for the stimulating discussions and for the friendship. I also would like to thank Ms. Tomomi Yamamoto and Ms. Chizue Naito for their kind help in the lab.

Last but not least, I would like to thank my family and relatives for their devoted support.

Fig. 1

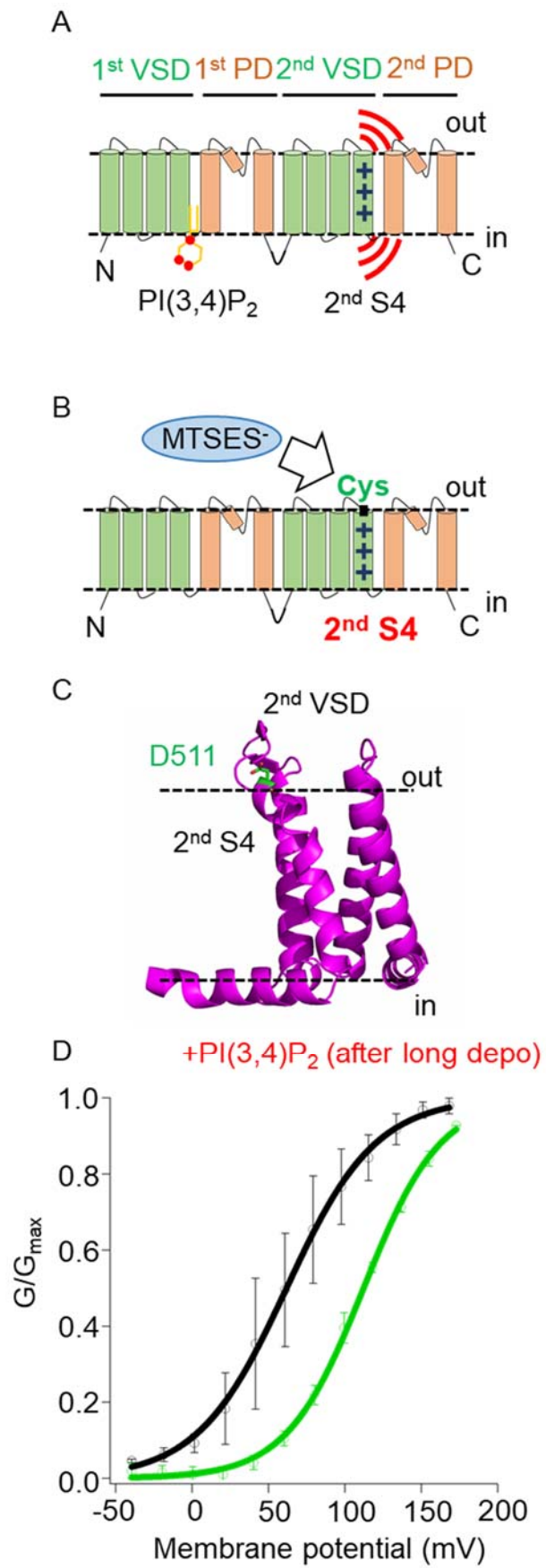


Fig. 1 Molecular structure of TPC3 and characterization of D511C-TPC3

A. A schematic presentation of TPC3 monomer. VSDs and PDs are colored in green and brown, respectively. PI(3,4)P₂ at the binding site in the 1st repeat and the arginine residues in the 2nd VSD are depicted. The voltage-dependent movement of the 2nd S4 is highlighted. **B.** A schematic presentation of the Cys-accessibility analysis using MTSES to detect structural change of the 2nd S4 of TPC3. **C.** A homology model of the 2nd VSD of XtTPC3 structure. It is based on the structure of mouse TPC1 (PDBID: 6C9A) (She et al., 2018). D511 which was mutated to Cys in this study is presented as sticks. **D.** The G-V relationships of TPC3 (WT, black) and D511C-TPC3 mutant (green) in the presence of PI(3,4)P₂. The membrane voltages for half maximum activation ($V_{1/2}$) are as follows. WT: 61.7 ± 19.1 mV ($n = 3$); D511C: 112.1 ± 2.5 mV ($n = 3$). The difference was statistically significant ($p = 0.02$ by unpaired t-test). The slope factors are as follows. WT: 25.3 ± 0.2 mV ($n = 3$); D511C: 25.2 ± 1.4 mV ($n = 3$).

Fig. 2

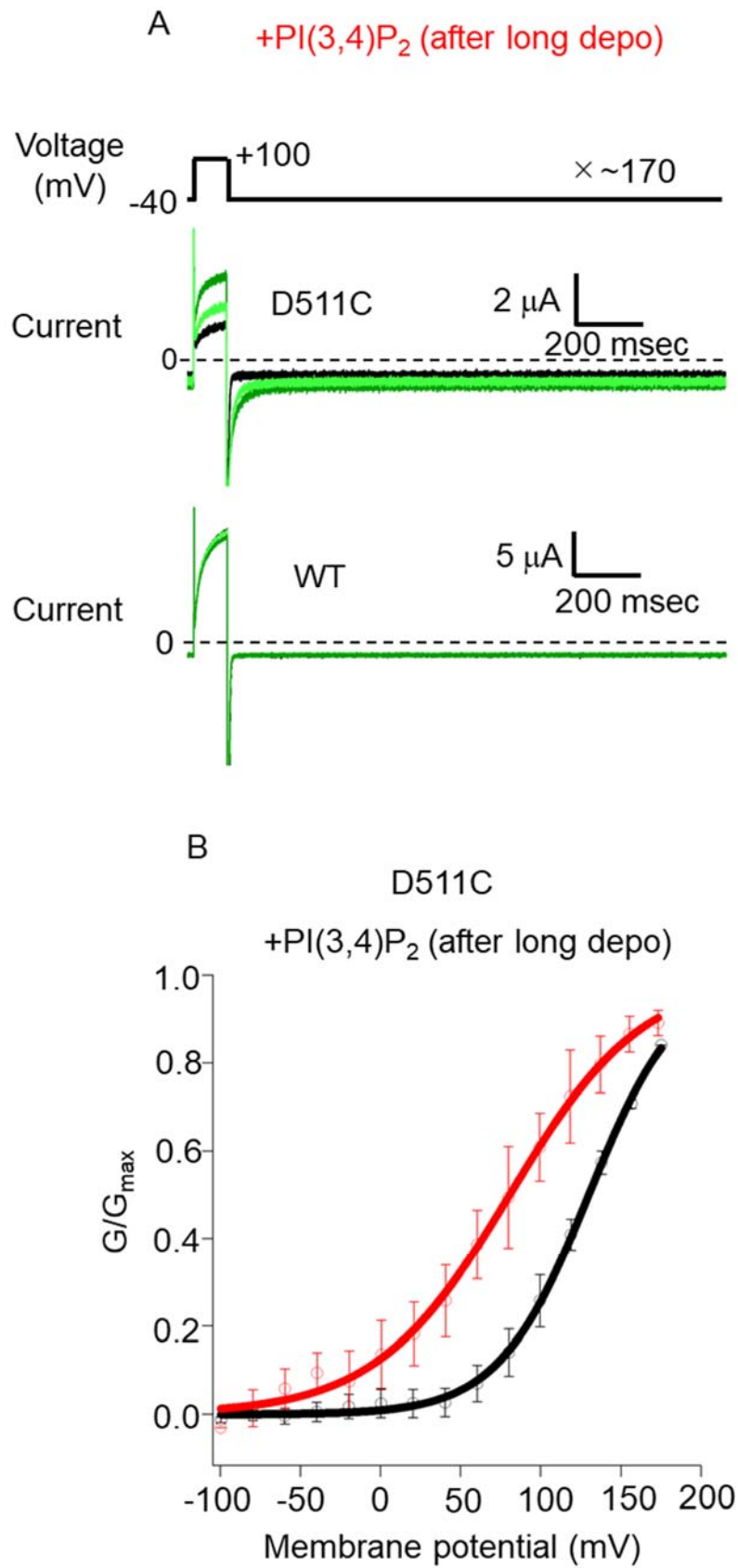


Fig. 2 Modification of D511C-TPC3 by MTSES

A. Representative TPC3 current traces recorded in the perfusion experiments of 0.5 mM MTSES. These experiments were performed in the presence of PI(3,4)P₂. The current traces at the beginning (black), in the middle (light green), at the end of the experiment (green) are shown. Upper panel shows recording of D511C-TPC3, lower panel shows that of wild type (WT) TPC3.

B. The G-V relationships of D511C-TPC3 after the modification without (black) or with 0.5 mM MTSES (red) in the presence of PI(3,4)P₂. V_{1/2s} are as follows. Without MTSES: 128.8 ± 2.2 mV (n = 4); with 0.5 mM MTSES: 86.3 ± 19.6 mV (n = 6). The difference was statistically significant (p = 0.005 by unpaired t-test). The slope factors are as follows. Without MTSES: 27.9 ± 4.8 mV (n = 4); with 0.5 mM MTSES: 45.6 ± 18.6 mV (n = 6).

Fig. 3

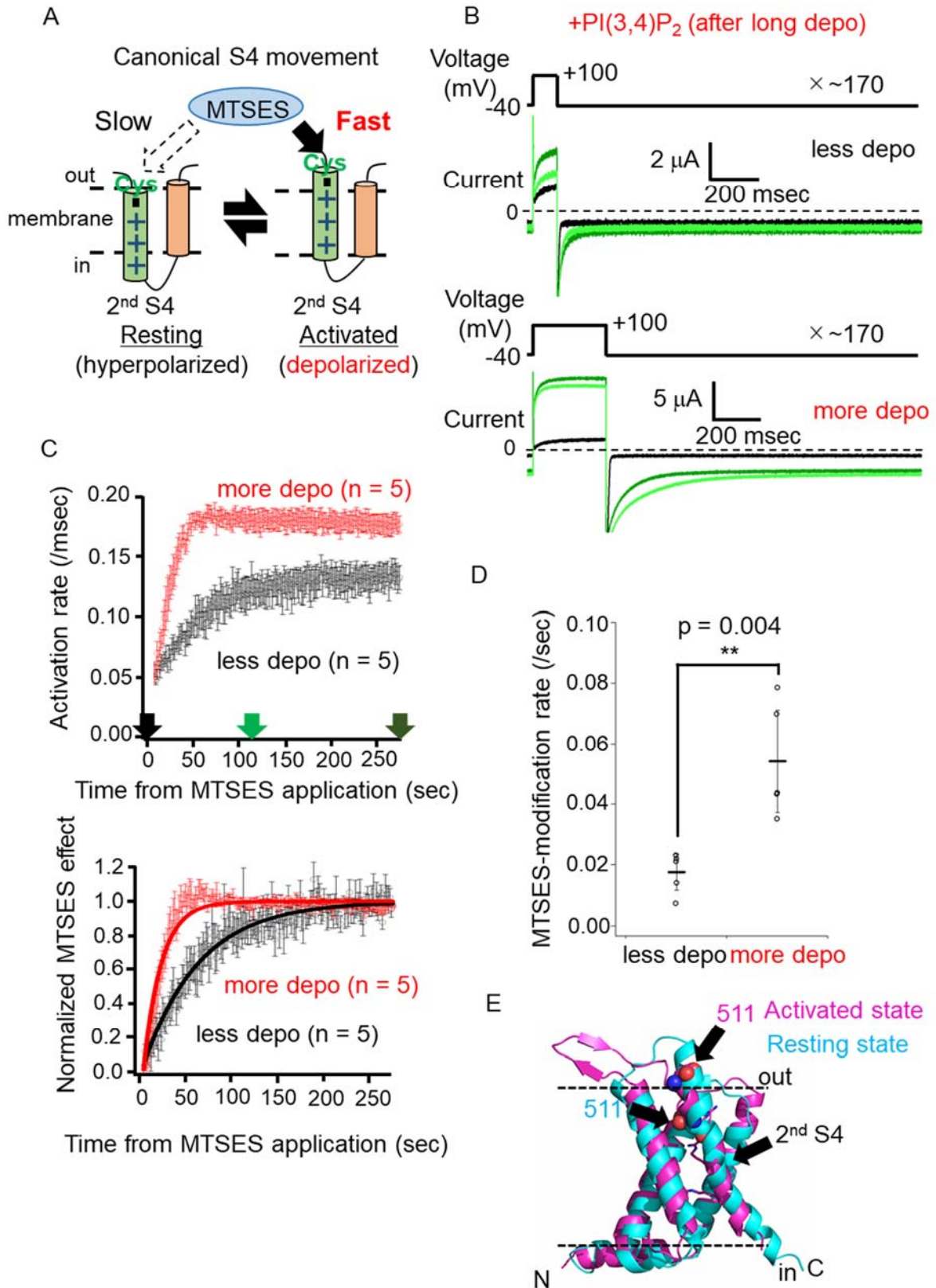


Fig. 3 Modification of D511C by MTSES is state-dependent.

A. A schematic view of the voltage dependence of the MTSES-modification rate due to the movement of the 2nd S4. **B.** Representative TPC3 current traces recorded in the presence of 0.5 mM MTSES using two protocols with different lengths of depolarization. These experiments were performed in the presence of PI(3,4)P₂. The traces are shown in the same manner as Fig. 2A. **C.** Upper: the time lapse change of the activation rates. Activation rates of TPC3 were obtained as described in Methods. The data in black are the results by the protocol with a short depolarization and the ones in red are those by the protocol with a longer depolarization. The arrows indicate the time when the traces in Fig. 3B were recorded (indicated by the same colors). lower: the time lapse change of the normalized MTSES effect (Methods). The color codes are the same as in upper panel. Circles show the obtained data and solid lines show the results of single exponential fit. Error bars show S.E.M (n = 5). **D.** Statistical comparison of the MTSES-modification rates obtained using two protocols. Less depolarized protocol: 0.018 ± 0.006 /sec (n = 5); More depolarized protocol: 0.054 ± 0.017 /sec (n = 5). (p = 0.004 by unpaired t-test) **E.** Homology models of the 2nd VSD of XtTPC3 structure in the resting and activated states. The model in the activated state (magenta) is based on the structure of mouse TPC1 (PDBID: 6C9A) (She et al., 2018). The model in the resting state (cyan) is based on the structure of Arabidopsis TPC1 (PDBID: 5E1J) (Guo et al., 2016). D511 which was mutated to Cys in this study is presented as spheres.

Fig. 4

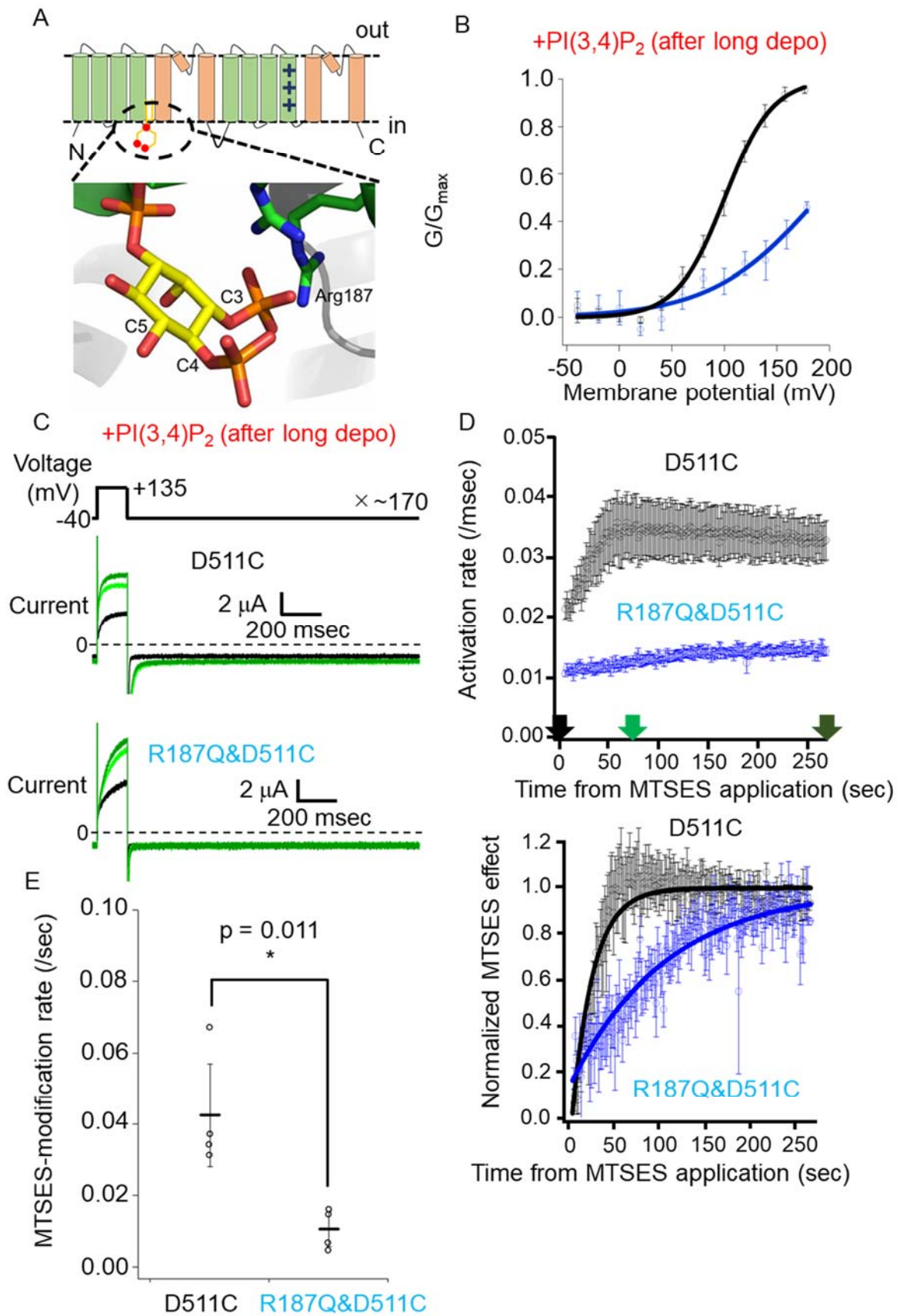


Fig. 4 R187Q mutation decelerates the MTSES-modification of D511C.

A. The model of the binding mode of PI(3,4)P₂ in the 1st repeat of XtTPC3. This model is based on the structure of mouse TPC1 (PDBID: 6C9A) (She et al., 2018). Arg187 which is mutated to Gln in this experiment and modeled PI(3,4)P₂ are depicted as sticks. **B.** The G-V relationships of D511C-TPC3 and R187Q&D511C-TPC3 mutants before modification by MTSES in the presence of PI(3,4)P₂. V_{1/2s} are as follows. D511C-TPC3: 100.5 ± 4.8 mV (n = 10); R187Q&D511C-TPC3: 180.0 ± 50.1 mV (n = 8). The difference was statistically significant (p < 0.001 by unpaired t-test). The slope factors are as follows. D511C-TPC3: 22.9 ± 2.8 mV (n = 10); R187Q&D511C-TPC3: 46.1 ± 20.9 mV (n = 8). **C.** Representative TPC3 current traces recorded in the presence of 0.5 mM MTSES. These experiments were performed in the presence of PI(3,4)P₂. The traces are shown in the same manner as Fig. 2A. **D.** Upper: the time lapse change of activation rates. The data in black are the results of D511C-TPC3 and the ones in blue are those of R187Q&D511C-TPC3. Lower: the time lapse change of the normalized MTSES effect (Methods). The color codes are the same as in the upper panel. These figures are shown in the same manner to Fig. 3C. Error bars show S.E.M (n = 4). **E.** Statistical comparison of the MTSES-modification rates of two constructs. D511C-TPC3: 0.043 ± 0.014 /sec (n = 4); R187Q&D511C-TPC3: 0.011 ± 0.005 /sec (n = 4). (p = 0.011 by unpaired t-test)

Fig. 5

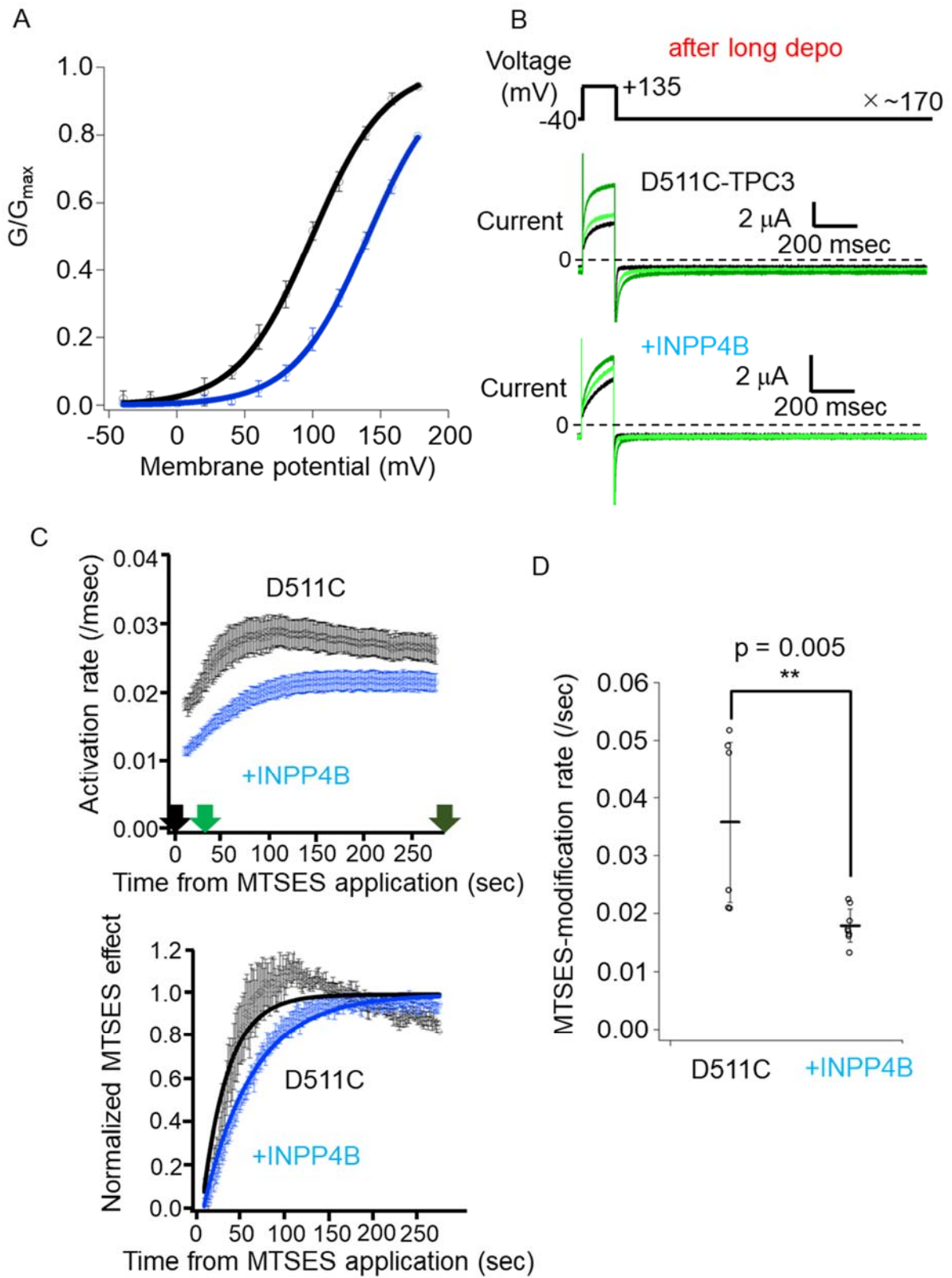


Fig. 5 INPP4B co-expression decelerates the MTSES-modification of D511C.

A. The G-V relationships of D511C-TPC3 with or without INPP4B before modification by MTSES after long depolarization. $V_{1/2S}$ are as follows. D511C-TPC3: 99.5 ± 3.4 mV (n = 6); D511C-TPC3+INPP4B: 140.4 ± 3.5 mV (n = 6). The difference was statistically significant ($p < 0.001$ by unpaired t-test). The slope factors are as follows. D511C-TPC3: 27.4 ± 2.9 mV (n = 6); D511C-TPC3+INPP4B: 27.4 ± 2.4 mV (n = 6). **B.** Representative TPC3 current traces recorded in the presence of 0.5 mM MTSES. These experiments were performed after long depolarization. The traces are shown in the same manner as Fig. 2A. **C.** Upper: the time lapse change of activation rates. The data in black are the results of D511C-TPC3 expressed alone and the ones in blue are those of D511C-TPC3 expressed with INPP4B. Lower: the time lapse change of the normalized MTSES effect (Methods). The color codes are the same as in the upper panel. These figures are shown in the same manner as Fig. 3C. Error bars show S.E.M (n = 6 for D511C, n = 8 for D511C+INPP4B). **D.** Statistical comparison of the MTSES-modification rates of D511C-TPC3 with or without INPP4B. D511C-TPC3: 0.036 ± 0.014 /sec (n = 6); D511C-TPC3+INPP4B: 0.018 ± 0.003 /sec (n = 8). ($p = 0.005$ by unpaired t-test)

Fig. 6

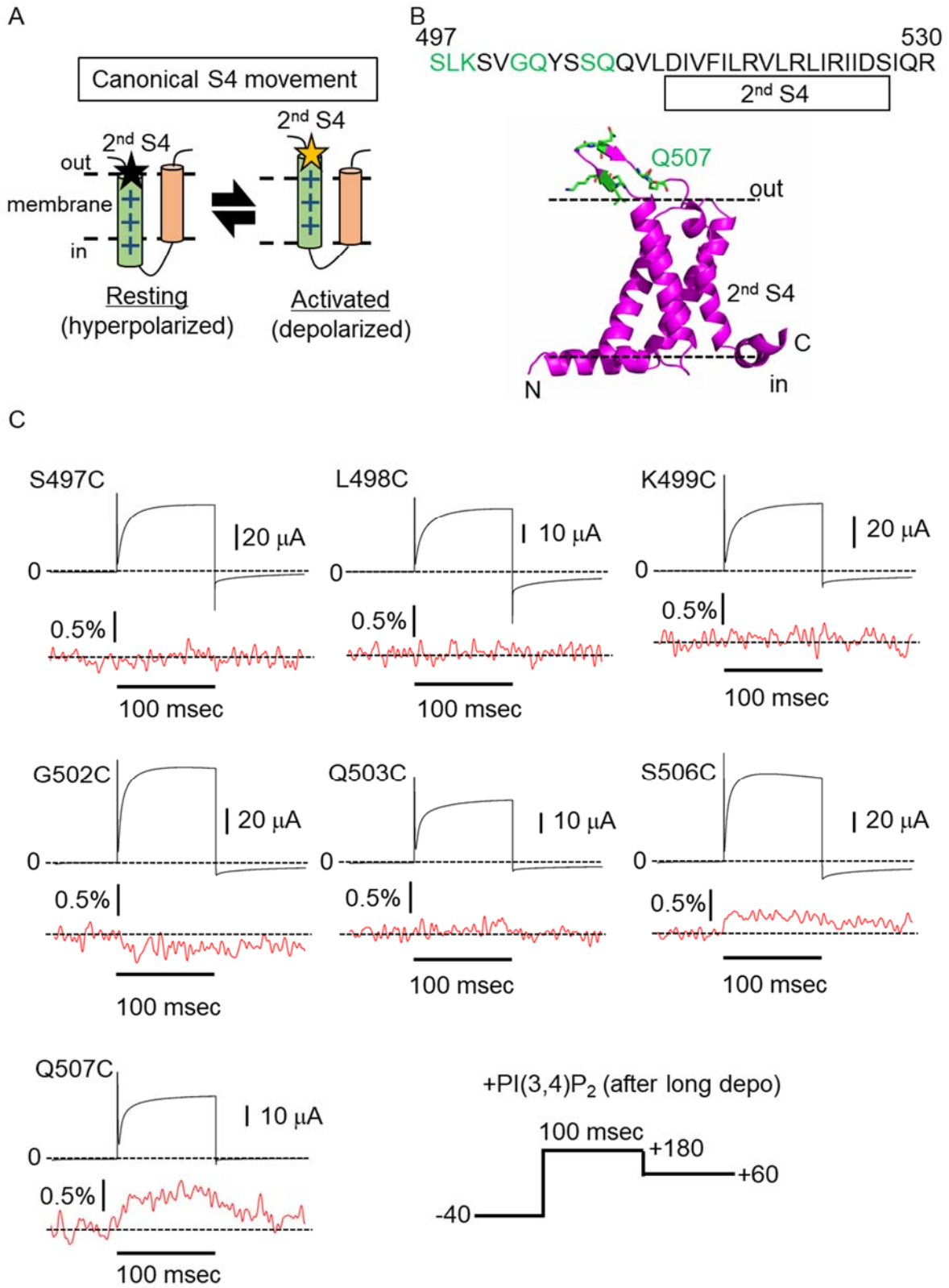


Fig. 6 Voltage clamp fluorometry of cysteine mutants of TPC3 labeled at the extracellular side of the 2nd S4

A. A schematic view of the voltage-dependent change of the fluorescent intensity in the 2nd S4.

B. Amino acid sequence around the 2nd S4 and homology model of the 2nd VSD structure. The numbers of the N-terminal and C-terminal amino acids are indicated in the sequence. The residues tested as candidates for Alexa-labeling are colored in green and shown as sticks in the model. Q507, the most successful position for Alexa-VCF, is highlighted in the model. The model is made in the same manner as that in Fig. 1C. **C.** Representative results showing TPC3 current traces (black) and fluorescence traces (red) of the 2nd S4 Alexa-constructs. These experiments were performed in the presence of PI(3,4)P₂. The voltage pulse is depicted at the bottom.

Fig. 7

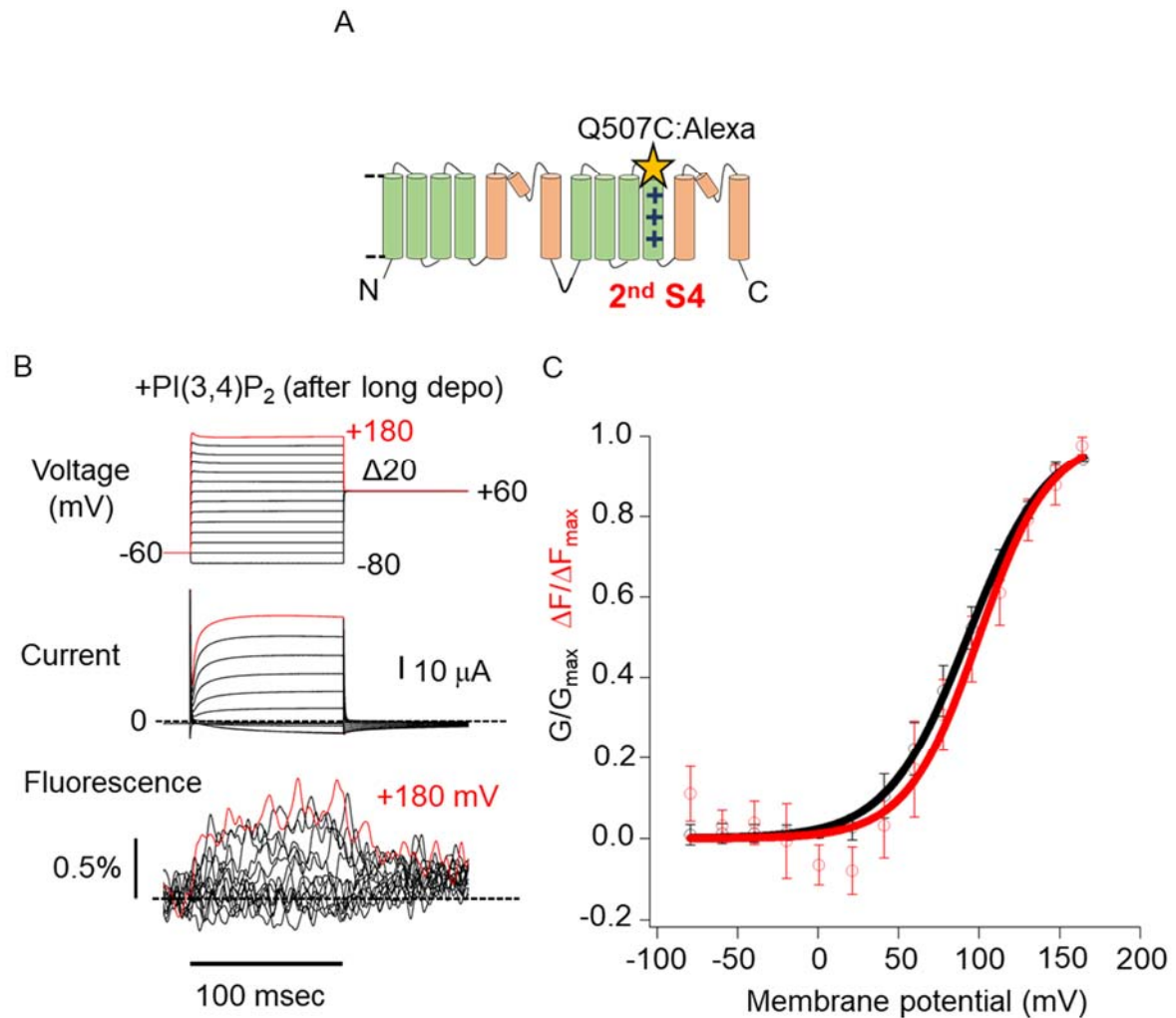


Fig. 7 G-V and ΔF -V relationships of Q507C:Alexa-TPC3

A. A schematic view of the position of Q507C. **B.** A representative result showing TPC3 current traces (middle) and fluorescence traces (bottom) of Q507C:Alexa-TPC3. These experiments were performed in the presence of PI(3,4)P₂. Traces shown in red are the depolarization pulse, current and fluorescent trace at +180 mV, respectively. **C.** The G-V (black) and ΔF -V (red) relationships of Q507C:Alexa-TPC3 in the presence of PI(3,4)P₂. $V_{1/2S}$ are as follows. G-V: 91.9 ± 6.7 mV; ΔF -V: 99.2 ± 8.8 mV ($n = 10$). The slope factors are as follows. G-V: 24.8 ± 3.7 mV; ΔF -V: 22.1 ± 4.1 mV ($n = 10$).

Fig. 8

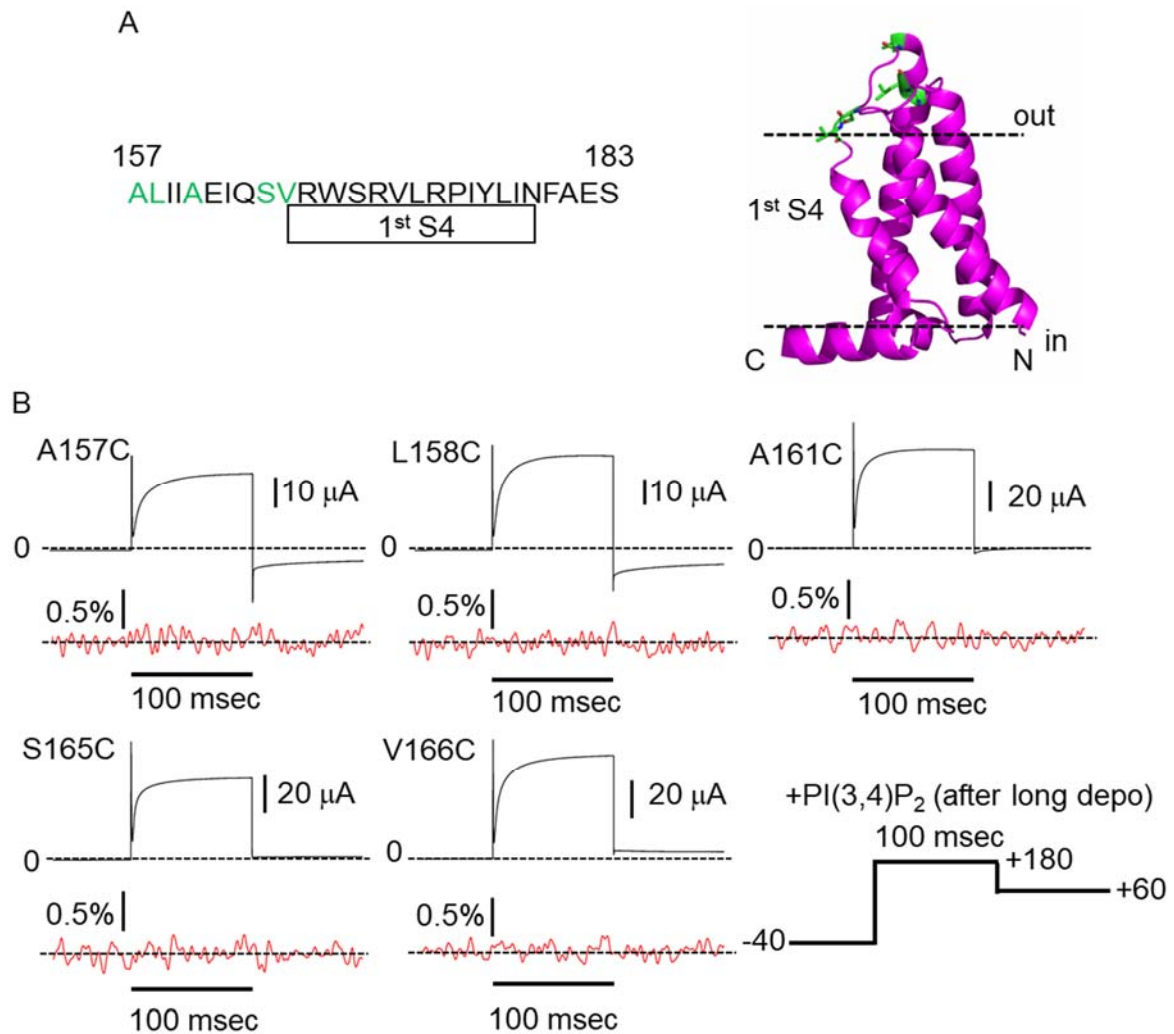


Fig. 8 Voltage clamp fluorometry of cysteine mutants of TPC3 labeled at the extracellular side of the 1st S4

A, Amino acid sequence around the 1st S4 and homology model of the 1st VSD structure. The numbers of the N-terminal and C-terminal amino acids are indicated in the sequence. The residues tested as candidates for Alexa-labeling are colored in green and shown as sticks in the model. The model is made in the same manner as that in Fig. 1C. **B**. Representative results showing TPC3 current traces (black) and fluorescence traces (red) of the 1st S4 Alexa-constructs. These experiments were performed in the presence of PI(3,4)P₂. The voltage pulse is depicted at the bottom.

Fig. 9

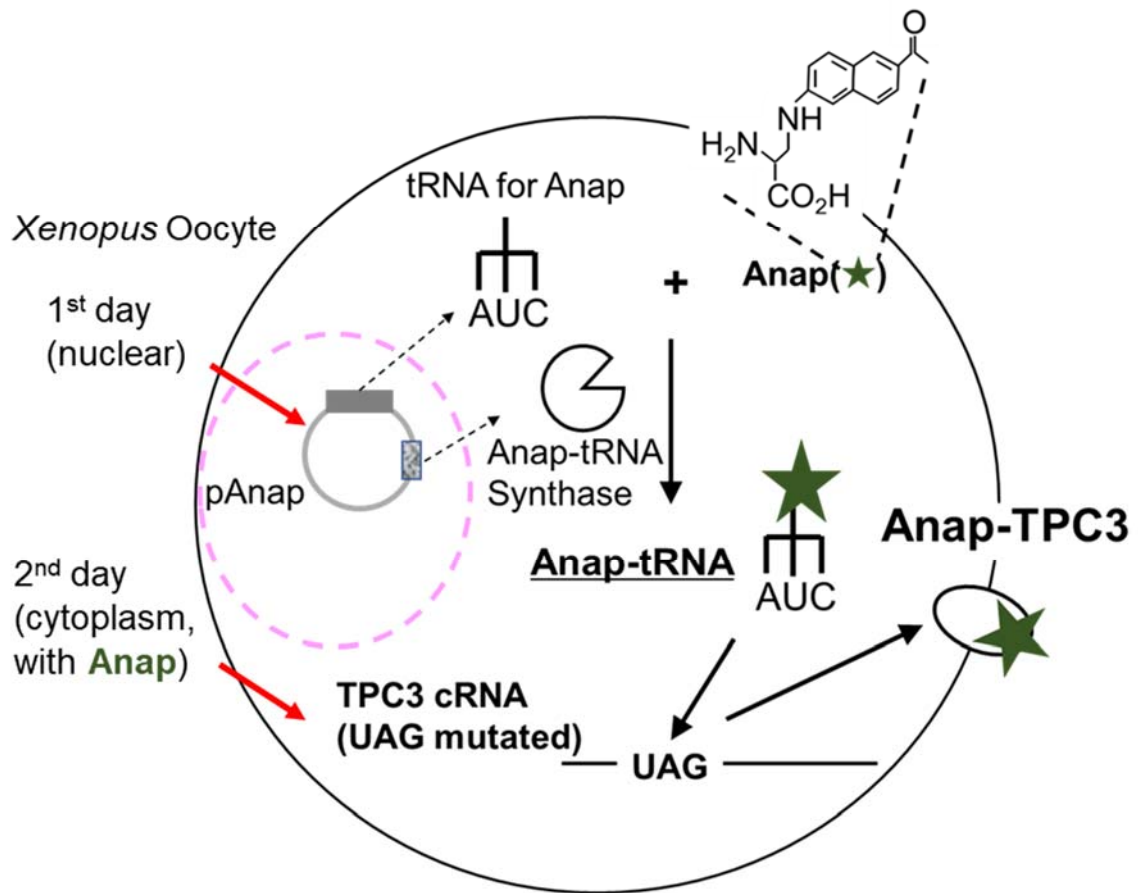


Fig. 9 A schematic explanation of the incorporation of Anap into the polypeptide chain of TPC3

Fig. 10

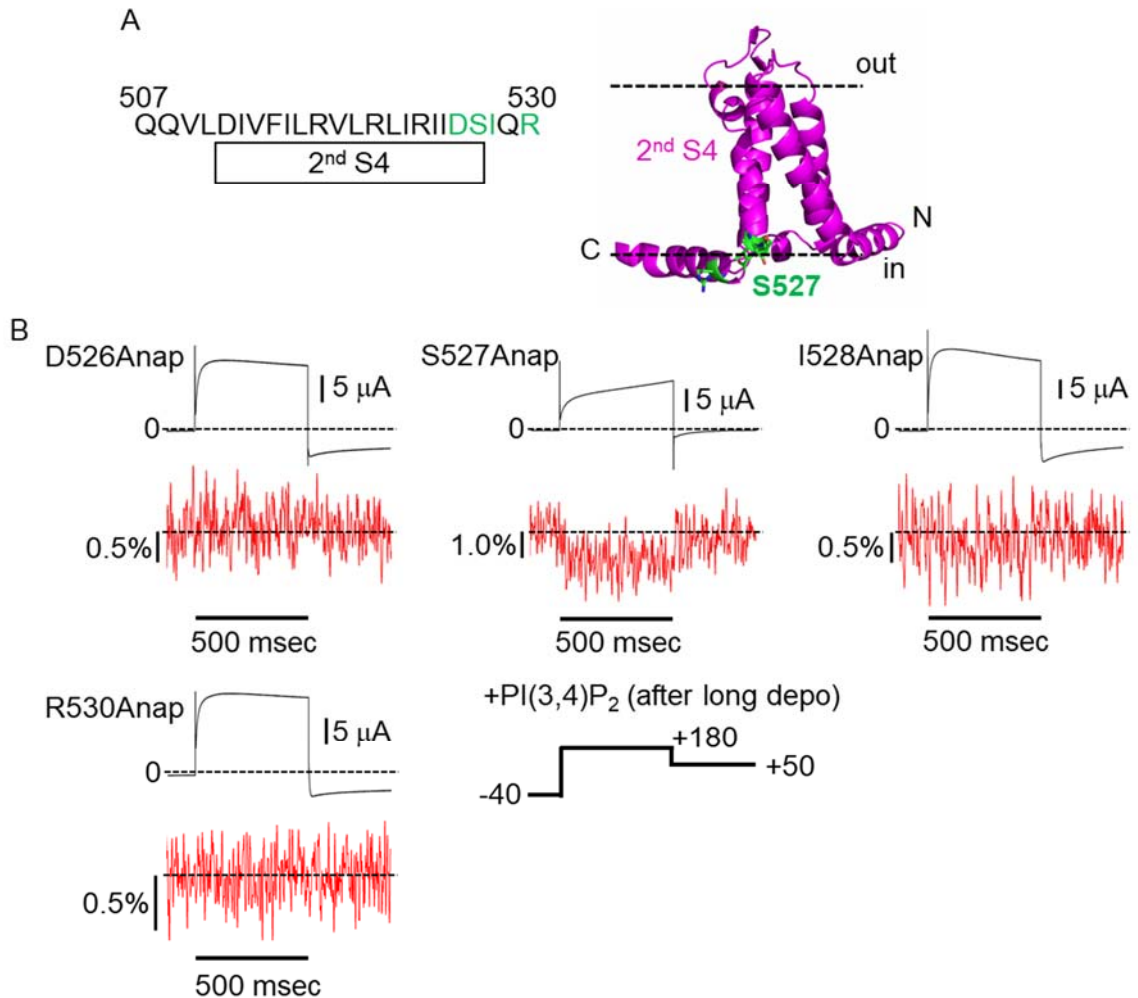


Fig. 10 Voltage clamp fluorometry of Anap mutants of TPC3 at the intracellular side of the 2nd S4

A. Amino acid sequence around the 2nd S4 and homology model of the 2nd VSD structure. The numbers of the N-terminal and C-terminal amino acids are indicated in the sequence. The residues tested as candidates for Anap-labeling are colored green and shown as sticks in the model. S527, the most successful position for Anap-VCF, is highlighted in the model. The model is made in the same manner as that in Fig. 1C. **B.** Representative results showing TPC3 current traces (black) and fluorescence traces (red) of the 2nd S4 Anap-constructs. These experiments were performed in the presence of PI(3,4)P₂. The voltage pulse is depicted at the bottom.

Fig. 11

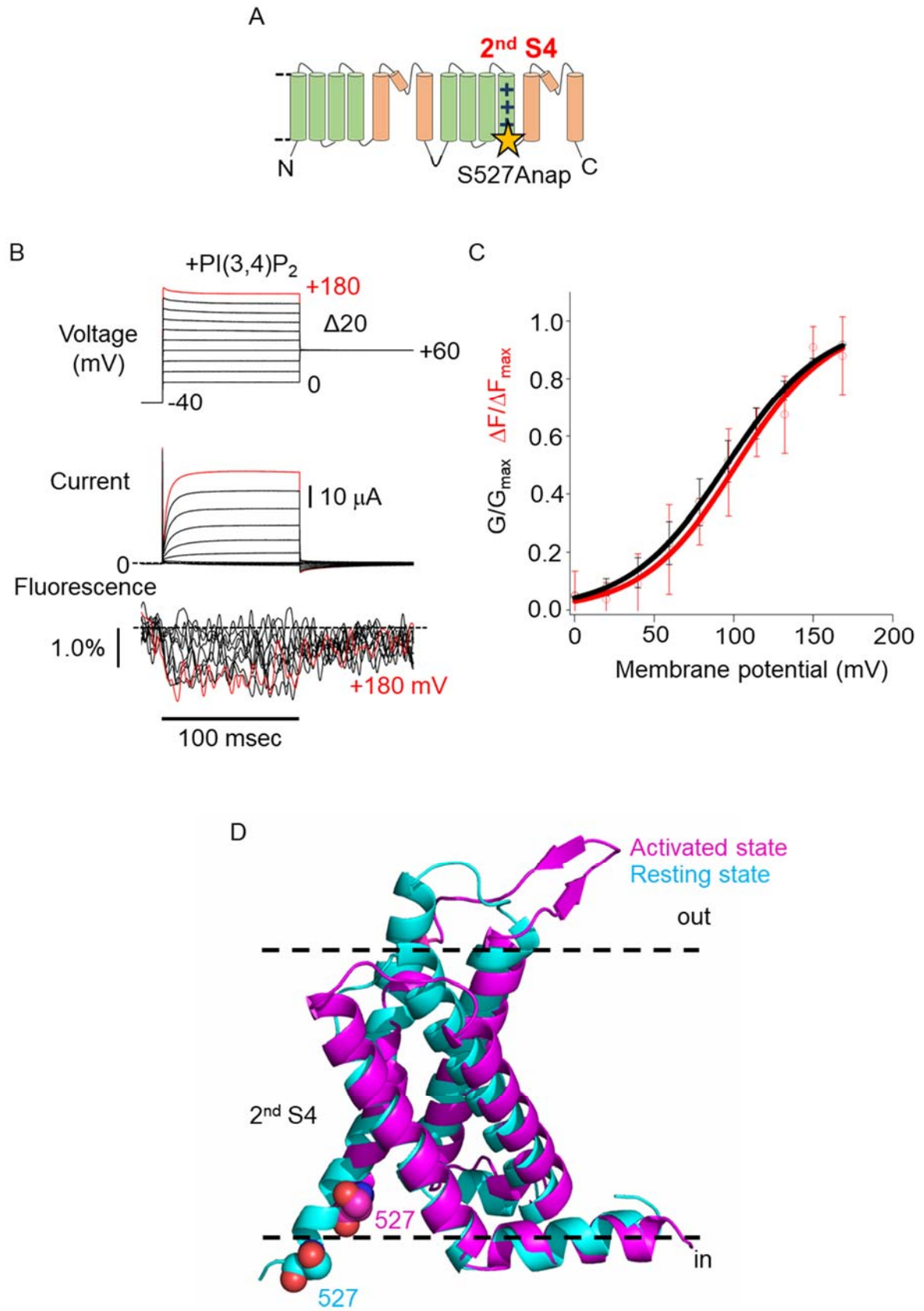


Fig. 11 G-V and ΔF -V relationships of S527Anap-TPC3

A. A schematic view of the position of S527Anap. **B.** A representative result showing TPC3 current traces (middle) and fluorescence traces (bottom) of S527Anap-TPC3. These experiments were performed in the presence of PI(3,4)P₂. Traces shown in red are the depolarization pulse, current and fluorescent trace at +180 mV, respectively. **C.** The G-V (black) and ΔF -V (red) relationships of S527Anap-TPC3 in the presence of PI(3,4)P₂. $V_{1/2S}$ are as follows. G-V: 93.5 ± 11.9 mV; ΔF -V: 119.0 ± 45.3 mV ($n = 7$). The slope factors are as follows. G-V: 30.2 ± 4.2 mV; ΔF -V: 34.1 ± 16.5 mV ($n = 7$). **D.** Homology models of the 2nd VSD of XtTPC3 structure in the resting and activated states. These models are the same as those in Fig. 3E. S527 which was mutated to Anap in this study is presented as spheres.

Fig. 12

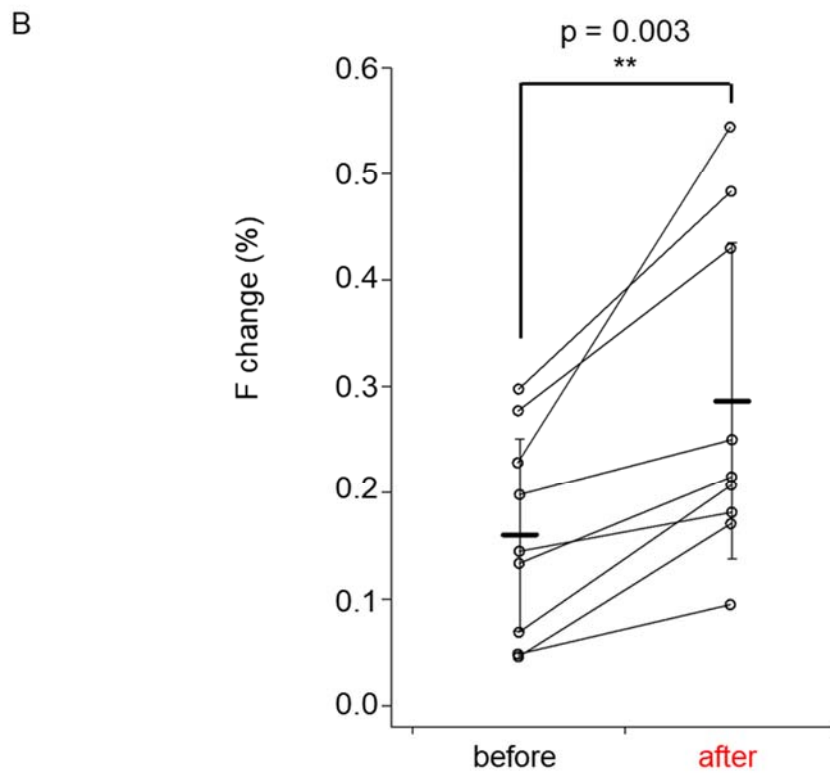
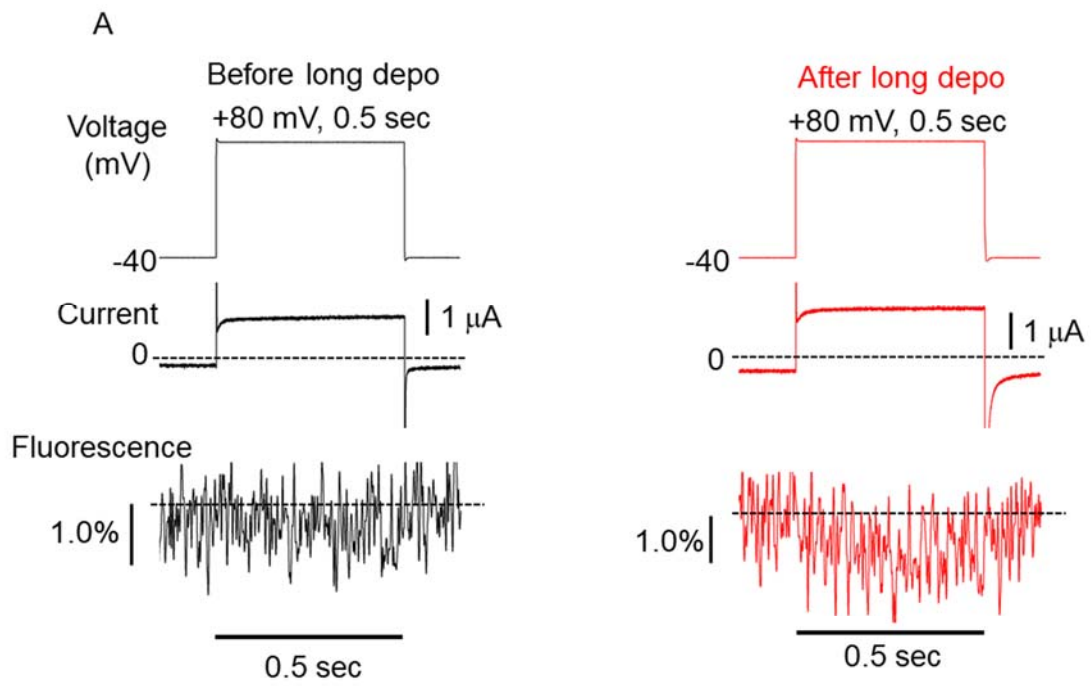


Fig. 12 Comparison of the F changes of S527Anap-TPC3 before and after long depolarization

A. A representative result showing S527Anap-TPC3 current traces and fluorescence traces before (black) and after (red) long depolarization. The long depolarization is expected to increase PI(3,4)P₂ concentration in the oocyte. These traces were recorded from the same oocyte. **B.** Statistical comparison of the F changes of S527Anap-TPC3 before and after long depolarization. The averages of the detected F changes are as follows. Before long depolarization: $0.16 \pm 0.09\%$; after long depolarization: $0.29 \pm 0.15\%$ (n = 9). (p = 0.003 by paired t-test)

Fig. 13

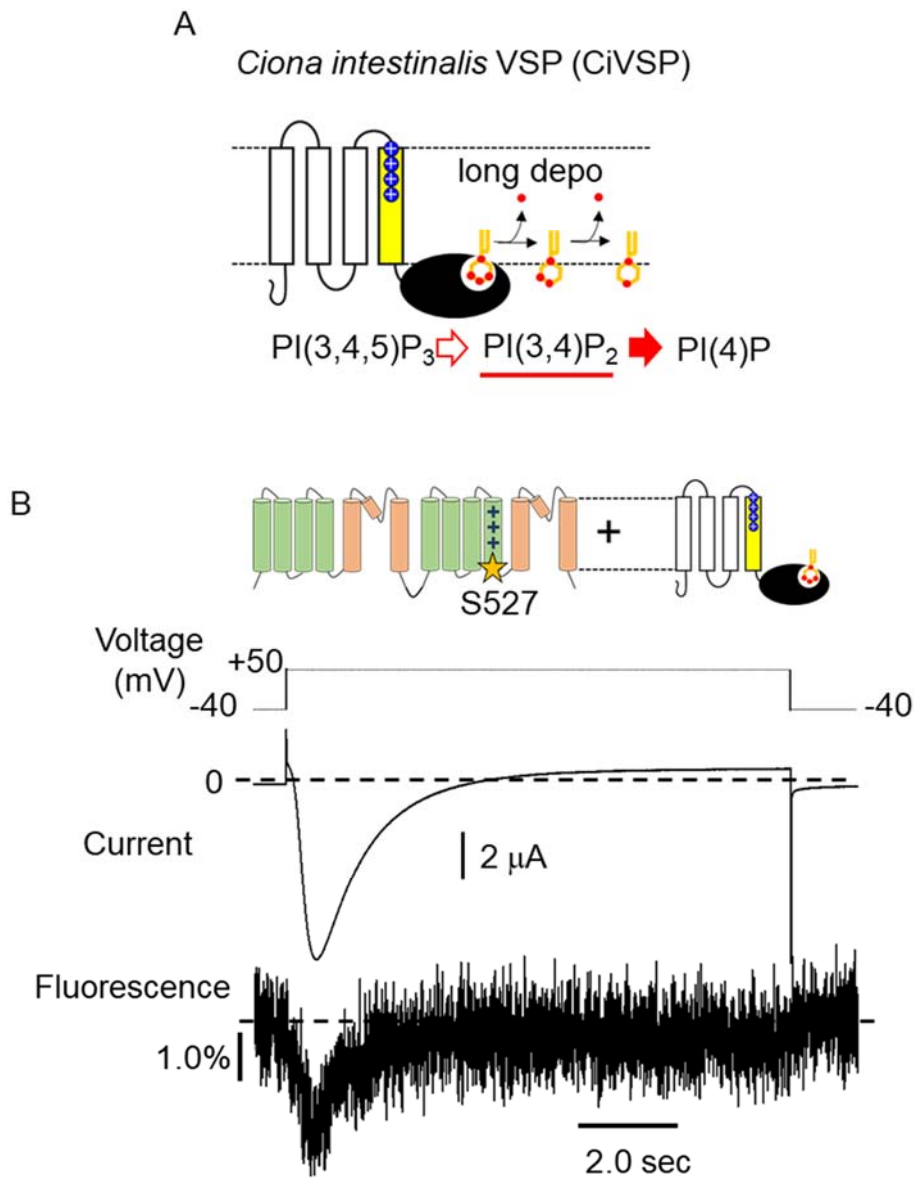


Fig. 13 Co-expression of CiVSP with S527Anap-TPC3 evokes a rapid and biphasic F change.

A. A schematic explanation of the enzymatic activity of *Ciona intestinalis* voltage-sensitive phosphatase (CiVSP). **B.** Representative result of the co-expression experiment of S527Anap-TPC3 with CiVSP.

Fig. 14

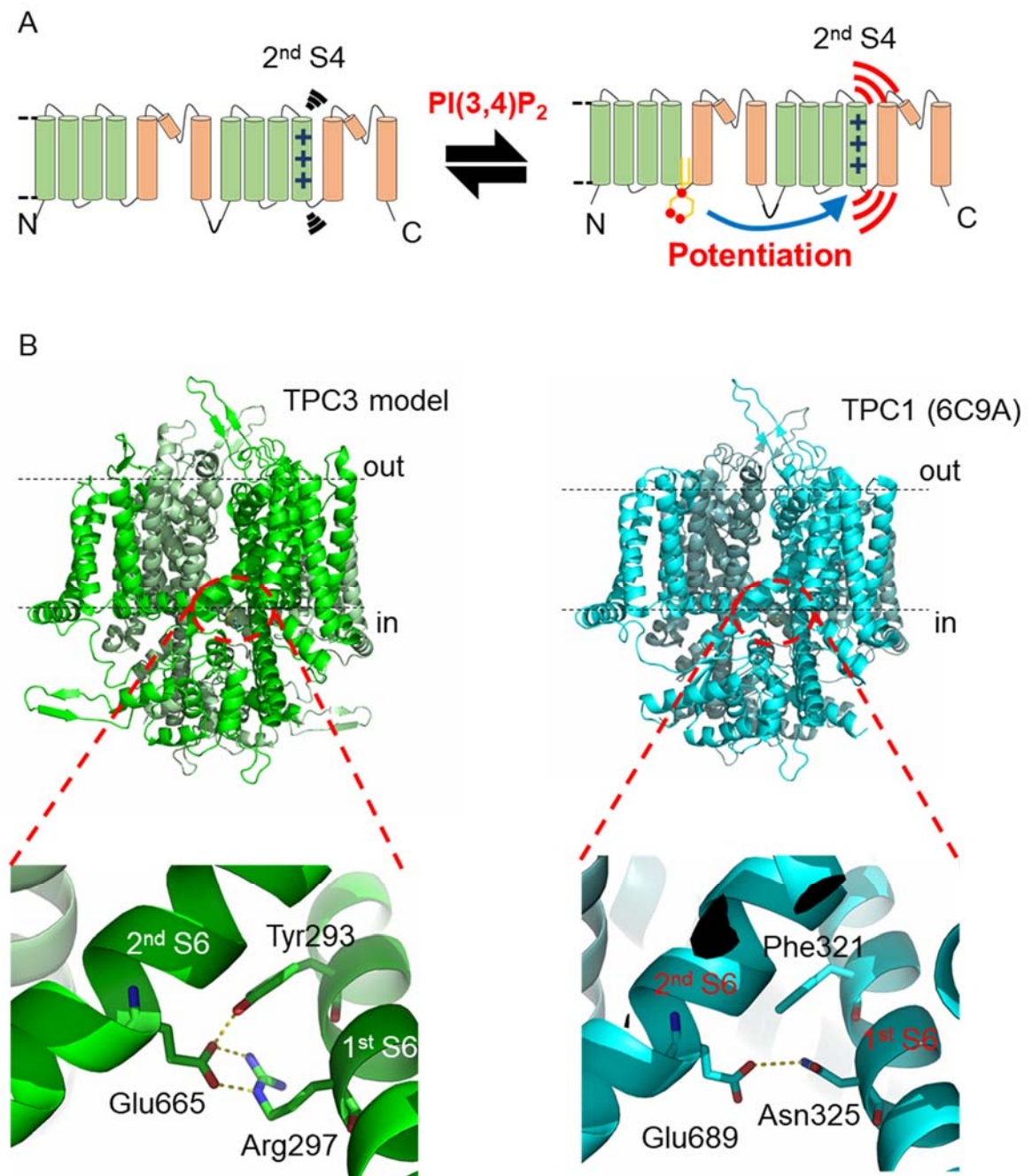


Fig. 14 The effect of PI(3,4)P₂ binding on the 2nd S4 via the inter-repeat linking of TPC3

A. A schematic explanation of the potentiation of the structural change of the 2nd S4 by PI(3,4)P₂ binding revealed by this study. **B.** A model of the inter-repeat linking specific for TPC3. The homology model of XtTPC3 structure (green) is based on the structure of mouse TPC1 (PDBID:6C9A) (She et al., 2018) shown on the right side (cyan). The inter-repeat linking is shown in below highlighting the residues important for this linking depicted as sticks. Possible hydrophilic and electrostatic interactions are shown as dotted lines. On the right side, corresponding residues of TPC1 are shown in the same manner for comparison.

References

- Aggarwal, S. K., MacKinnon, R. (1996). Contribution of the S4 segment to gating charge in the Shaker K⁺ channel. *Neuron*, 16(6), 1169-1177. doi: 10.1016/s0896-6273(00)80143-9
- Amey, J. S., O'Reilly, A. O., Burton, M. J., Puinean, A. M., Mellor, I. R., Duce, I. R., Field, L. M., Wallace, B. A., Williamson, M. S., Davies, T. G. (2015). An evolutionarily-unique heterodimeric voltage-gated cation channel found in aphids. *FEBS Lett*, 589(5), 598-607. doi: 10.1016/j.febslet.2015.01.020
- Armstrong, C. M., Bezanilla, F. (1974). Charge movement associated with the opening and closing of the activation gates of the Na channels. *J Gen Physiol*, 63(5), 533-552. doi: 10.1085/jgp.63.5.533
- Arnold, K., Bordoli, L., Kopp, J., Schwede, T. (2006). The SWISS-MODEL workspace: a web-based environment for protein structure homology modelling. *Bioinformatics*, 22(2), 195-201. doi: 10.1093/bioinformatics/bti770
- Ashcroft, F. M. (2006). From molecule to malady. *Nature*, 440(7083), 440-447. doi: 10.1038/nature04707
- Baker, O. S., Larsson, H. P., Mannuzzu, L. M., Isacoff, E. Y. (1998). Three transmembrane conformations and sequence-dependent displacement of the S4 domain in shaker K⁺ channel gating. *Neuron*, 20(6), 1283-1294. doi: 10.1016/s0896-6273(00)80507-3
- Biasini, M., Bienert, S., Waterhouse, A., Arnold, K., Studer, G., Schmidt, T., Kiefer, F., Gallo Cassarino, T., Bertoni, M., Bordoli, L., Schwede, T. (2014). SWISS-MODEL: modelling protein tertiary and quaternary structure using evolutionary information. *Nucleic Acids Res*, 42(Web Server issue), W252-258. doi: 10.1093/nar/gku340
- Blunck, R., Starace, D. M., Correa, A. M., Bezanilla, F. (2004). Detecting rearrangements of shaker and NaChBac in real-time with fluorescence spectroscopy in patch-clamped

- mammalian cells. *Biophys J*, 86(6), 3966-3980. doi: 10.1529/biophysj.103.034512
- Calcraft, P. J., Ruas, M., Pan, Z., Cheng, X., Arredouani, A., Hao, X., Tang, J., Rietdorf, K., Teboul, L., Chuang, K. T., Lin, P., Xiao, R., Wang, C., Zhu, Y., Lin, Y., Wyatt, C. N., Parrington, J., Ma, J., Evans, A. M., Galione, A., Zhu, M. X. (2009). NAADP mobilizes calcium from acidic organelles through two-pore channels. *Nature*, 459(7246), 596-600. doi: 10.1038/nature08030
- Cang, C., Aranda, K., Ren, D. (2014). A non-inactivating high-voltage-activated two-pore Na⁺ channel that supports ultra-long action potentials and membrane bistability. *Nat Commun*, 5, 5015. doi: 10.1038/ncomms6015
- Cang, C., Bekele, B., Ren, D. (2014). The voltage-gated sodium channel TPC1 confers endolysosomal excitability. *Nat Chem Biol*, 10(6), 463-469. doi: 10.1038/nchembio.1522
- Cang, C., Zhou, Y., Navarro, B., Seo, Y. J., Aranda, K., Shi, L., Battaglia-Hsu, S., Nissim, I., Clapham, D. E., Ren, D. (2013). mTOR regulates lysosomal ATP-sensitive two-pore Na(+) channels to adapt to metabolic state. *Cell*, 152(4), 778-790. doi: 10.1016/j.cell.2013.01.023
- Catterall, W. A. (2000). From ionic currents to molecular mechanisms: the structure and function of voltage-gated sodium channels. *Neuron*, 26(1), 13-25. doi: 10.1016/s0896-6273(00)81133-2
- Cha, A., Bezanilla, F. (1997). Characterizing voltage-dependent conformational changes in the Shaker K⁺ channel with fluorescence. *Neuron*, 19(5), 1127-1140. doi: 10.1016/s0896-6273(00)80403-1
- Dickinson, M. S., Myasnikov, A., Eriksen, J., Poweleit, N., Stroud, R. M. (2020). Resting state structure of the hyperdepolarization activated two-pore channel 3. *Proc Natl Acad Sci U S A*, 117(4), 1988-1993. doi: 10.1073/pnas.1915144117
- Doyle, D. A., Morais Cabral, J., Pfuetzner, R. A., Kuo, A., Gulbis, J. M., Cohen, S. L., Chait,

- B. T., MacKinnon, R. (1998). The structure of the potassium channel: molecular basis of K⁺ conduction and selectivity. *Science*, 280(5360), 69-77. doi: 10.1126/science.280.5360.69
- Fruman, D. A., Chiu, H., Hopkins, B. D., Bagrodia, S., Cantley, L. C., Abraham, R. T. (2017). The PI3K Pathway in Human Disease. *Cell*, 170(4), 605-635. doi: 10.1016/j.cell.2017.07.029
- García-Rúa, V., Feijóo-Bandín, S., Rodríguez-Penas, D., Mosquera-Leal, A., Abu-Assi, E., Beiras, A., María Seoane, L., Lear, P., Parrington, J., Portolés, M., Roselló-Lletí, E., Rivera, M., Gualillo, O., Parra, V., Hill, J. A., Rothermel, B., González-Juanatey, J. R., Lago, F. (2016). Endolysosomal two-pore channels regulate autophagy in cardiomyocytes. *J Physiol*, 594(11), 3061-3077. doi: 10.1113/jp271332
- Grimm, S. S., Isacoff, E. Y. (2016). Allosteric substrate switching in a voltage-sensing lipid phosphatase. *Nat Chem Biol*, 12(4), 261-267. doi: 10.1038/nchembio.2022
- Guo, J., Zeng, W., Chen, Q., Lee, C., Chen, L., Yang, Y., Cang, C., Ren, D., Jiang, Y. (2016). Structure of the voltage-gated two-pore channel TPC1 from *Arabidopsis thaliana*. *Nature*, 531(7593), 196-201. doi: 10.1038/nature16446
- Guo, J., Zeng, W., Jiang, Y. (2017). Tuning the ion selectivity of two-pore channels. *Proc Natl Acad Sci U S A*, 114(5), 1009-1014. doi: 10.1073/pnas.1616191114
- Hebeisen, S., Fahlke, C. (2005). Carboxy-terminal truncations modify the outer pore vestibule of muscle chloride channels. *Biophys J*, 89(3), 1710-1720. doi: 10.1529/biophysj.104.056093
- Heinemann, S. H., Terlau, H., Stühmer, W., Imoto, K., Numa, S. (1992). Calcium channel characteristics conferred on the sodium channel by single mutations. *Nature*, 356(6368), 441-443. doi: 10.1038/356441a0
- Hille, B. (2001). Ion Channels of Excitable Membranes (Third Edition). *Sunderland: Sinauer Associates Inc.*

- Kalstrup, T., Blunck, R. (2013). Dynamics of internal pore opening in K(V) channels probed by a fluorescent unnatural amino acid. *Proc Natl Acad Sci U S A*, *110*(20), 8272-8277. doi: 10.1073/pnas.1220398110
- Kintzer, A. F., Green, E. M., Dominik, P. K., Bridges, M., Armache, J. P., Deneka, D., Kim, S. S., Hubbell, W., Kossiakoff, A. A., Cheng, Y., Stroud, R. M. (2018). Structural basis for activation of voltage sensor domains in an ion channel TPC1. *Proc Natl Acad Sci U S A*, *115*(39), E9095-E9104. doi: 10.1073/pnas.1805651115
- Kintzer, A. F., Stroud, R. M. (2016). Structure, inhibition and regulation of two-pore channel TPC1 from *Arabidopsis thaliana*. *Nature*, *531*(7593), 258-262. doi: 10.1038/nature17194
- Kurokawa, T., Takasuga, S., Sakata, S., Yamaguchi, S., Horie, S., Homma, K. J., Sasaki, T., Okamura, Y. (2012). 3' Phosphatase activity toward phosphatidylinositol 3,4-bisphosphate [PI(3,4)P₂] by voltage-sensing phosphatase (VSP). *Proc Natl Acad Sci U S A*, *109*(25), 10089-10094. doi: 10.1073/pnas.1203799109
- Larsson, H. P., Baker, O. S., Dhillon, D. S., Isacoff, E. Y. (1996). Transmembrane movement of the shaker K⁺ channel S4. *Neuron*, *16*(2), 387-397. doi: 10.1016/s0896-6273(00)80056-2
- Lee, H. S., Guo, J., Lemke, E. A., Dimla, R. D., Schultz, P. G. (2009). Genetic incorporation of a small, environmentally sensitive, fluorescent probe into proteins in *Saccharomyces cerevisiae*. *J Am Chem Soc*, *131*(36), 12921-12923. doi: 10.1021/ja904896s
- Li, M., Kawate, T., Silberberg, S. D., Swartz, K. J. (2010). Pore-opening mechanism in trimeric P2X receptor channels. *Nat Commun*, *1*(4), 44. doi: 10.1038/ncomms1048
- Lin, P. H., Duann, P., Komazaki, S., Park, K. H., Li, H., Sun, M., Sermersheim, M., Gumpper, K., Parrington, J., Galione, A., Evans, A. M., Zhu, M. X., Ma, J. (2015). Lysosomal two-pore channel subtype 2 (TPC2) regulates skeletal muscle autophagic signaling. *J Biol Chem*, *290*(6), 3377-3389. doi: 10.1074/jbc.M114.608471

- Long, S. B., Campbell, E. B., Mackinnon, R. (2005). Voltage sensor of Kv1.2: structural basis of electromechanical coupling. *Science*, 309(5736), 903-908. doi: 10.1126/science.1116270
- MacKinnon, R. (1995). Pore loops: an emerging theme in ion channel structure. *Neuron*, 14(5), 889-892. doi: 10.1016/0896-6273(95)90327-5
- Mannuzzu, L. M., Moronne, M. M., Isacoff, E. Y. (1996). Direct physical measure of conformational rearrangement underlying potassium channel gating. *Science*, 271(5246), 213-216. doi: 10.1126/science.271.5246.213
- Mori, Y., Friedrich, T., Kim, M. S., Mikami, A., Nakai, J., Ruth, P., Bosse, E., Hofmann, F., Flockerzi, V., Furuichi, T., et al. (1991). Primary structure and functional expression from complementary DNA of a brain calcium channel. *Nature*, 350(6317), 398-402. doi: 10.1038/350398a0
- Nakajo, K., Kubo, Y. (2007). KCNE1 and KCNE3 stabilize and/or slow voltage sensing S4 segment of KCNQ1 channel. *J Gen Physiol*, 130(3), 269-281. doi: 10.1085/jgp.200709805
- Nakajo, K., Kubo, Y. (2014). Steric hindrance between S4 and S5 of the KCNQ1/KCNE1 channel hampers pore opening. *Nat Commun*, 5, 4100. doi: 10.1038/ncomms5100
- Noda, M., Shimizu, S., Tanabe, T., Takai, T., Kayano, T., Ikeda, T., Takahashi, H., Nakayama, H., Kanaoka, Y., Minamino, N., et al. (1984). Primary structure of Electrophorus electricus sodium channel deduced from cDNA sequence. *Nature*, 312(5990), 121-127. doi: 10.1038/312121a0
- Papazian, D. M., Schwarz, T. L., Tempel, B. L., Jan, Y. N., Jan, L. Y. (1987). Cloning of genomic and complementary DNA from Shaker, a putative potassium channel gene from *Drosophila*. *Science*, 237(4816), 749-753. doi: 10.1126/science.2441470
- Peiter, E., Maathuis, F. J., Mills, L. N., Knight, H., Pelloux, J., Hetherington, A. M., Sanders, D. (2005). The vacuolar Ca²⁺-activated channel TPC1 regulates germination and

- stomatal movement. *Nature*, 434(7031), 404-408. doi: 10.1038/nature03381
- Penny, C. J., Rahman, T., Sula, A., Miles, A. J., Wallace, B. A., Patel, S. (2016). Isolated pores dissected from human two-pore channel 2 are functional. *Sci Rep*, 6, 38426. doi: 10.1038/srep38426
- Pless, S. A., Lynch, J. W. (2008). Illuminating the structure and function of Cys-loop receptors. *Clin Exp Pharmacol Physiol*, 35(10), 1137-1142. doi: 10.1111/j.1440-1681.2008.04954.x
- Rahman, T., Cai, X., Brailoiu, G. C., Abood, M. E., Brailoiu, E., Patel, S. (2014). Two-pore channels provide insight into the evolution of voltage-gated Ca²⁺ and Na⁺ channels. *Sci Signal*, 7(352), ra109. doi: 10.1126/scisignal.2005450
- Ramos, I., Reich, A., Wessel, G. M. (2014). Two-pore channels function in calcium regulation in sea star oocytes and embryos. *Development*, 141(23), 4598-4609. doi: 10.1242/dev.113563
- Sakata, S., Jinno, Y., Kawanabe, A., Okamura, Y. (2016). Voltage-dependent motion of the catalytic region of voltage-sensing phosphatase monitored by a fluorescent amino acid. *Proc Natl Acad Sci U S A*, 113(27), 7521-7526. doi: 10.1073/pnas.1604218113
- Sakurai, Y., Kolokoltsov, A. A., Chen, C. C., Tidwell, M. W., Bauta, W. E., Klugbauer, N., Grimm, C., Wahl-Schott, C., Biel, M., Davey, R. A. (2015). Ebola virus. Two-pore channels control Ebola virus host cell entry and are drug targets for disease treatment. *Science*, 347(6225), 995-998. doi: 10.1126/science.1258758
- Seoh, S. A., Sigg, D., Papazian, D. M., Bezanilla, F. (1996). Voltage-sensing residues in the S2 and S4 segments of the Shaker K⁺ channel. *Neuron*, 16(6), 1159-1167. doi: 10.1016/s0896-6273(00)80142-7
- She, J., Guo, J., Chen, Q., Zeng, W., Jiang, Y., Bai, X. C. (2018). Structural insights into the voltage and phospholipid activation of the mammalian TPC1 channel. *Nature*, 556(7699), 130-134. doi: 10.1038/nature26139

- She, J., Zeng, W., Guo, J., Chen, Q., Bai, X. C., Jiang, Y. (2019). Structural mechanisms of phospholipid activation of the human TPC2 channel. *Elife*, 8. doi: 10.7554/eLife.45222
- Shimomura, T., Kubo, Y. (2019). Phosphoinositides modulate the voltage dependence of two-pore channel 3. *J Gen Physiol*, 151(8), 986-1006. doi: 10.1085/jgp.201812285
- Strong, M., Chandy, K. G., Gutman, G. A. (1993). Molecular evolution of voltage-sensitive ion channel genes: on the origins of electrical excitability. *Mol Biol Evol*, 10(1), 221-242. doi: 10.1093/oxfordjournals.molbev.a039986
- Talwar, S., Lynch, J. W. (2015). Investigating ion channel conformational changes using voltage clamp fluorometry. *Neuropharmacology*, 98, 3-12. doi: 10.1016/j.neuropharm.2015.03.018
- Vaid, M., Horne, A., Claydon, T., Fedida, D. (2009). Rapid outer pore movements after opening in a KV1 potassium channel are revealed by TMRM fluorescence from the S3-S4 linker, and modulated by extracellular potassium. *Channels (Austin)*, 3(1), 3-5. doi: 10.4161/chan.3.1.7369
- Wang, G., Shahidullah, M., Rocha, C. A., Strang, C., Pfaffinger, P. J., Covarrubias, M. (2005). Functionally active t1-t1 interfaces revealed by the accessibility of intracellular thiolate groups in kv4 channels. *J Gen Physiol*, 126(1), 55-69. doi: 10.1085/jgp.200509288
- Wang, X., Zhang, X., Dong, X. P., Samie, M., Li, X., Cheng, X., Goschka, A., Shen, D., Zhou, Y., Harlow, J., Zhu, M. X., Clapham, D. E., Ren, D., Xu, H. (2012). TPC proteins are phosphoinositide-activated sodium-selective ion channels in endosomes and lysosomes. *Cell*, 151(2), 372-383. doi: 10.1016/j.cell.2012.08.036
- Xu, H., Ren, D. (2015). Lysosomal physiology. *Annu Rev Physiol*, 77, 57-80. doi: 10.1146/annurev-physiol-021014-071649
- Yang, N., George, A. L., Jr., Horn, R. (1996). Molecular basis of charge movement in voltage-gated sodium channels. *Neuron*, 16(1), 113-122. doi: 10.1016/s0896-6273(00)80028-8
- Yu, F. H., Catterall, W. A. (2004). The VGL-chanome: a protein superfamily specialized for

electrical signaling and ionic homeostasis. *Sci STKE*, 2004(253), re15. doi:
10.1126/stke.2532004re15